

UNCLASSIFIED

AD NUMBER

AD837231

LIMITATION CHANGES

TO:

Approved for public release; distribution is unlimited.

FROM:

Distribution authorized to U.S. Gov't. agencies and their contractors; Critical Technology; JUL 1968. Other requests shall be referred to Air Force Technical Application Center, VELA Seismological Center, Washington, DC 20333. This document contains export-controlled technical data.

AUTHORITY

usaf ltr 1972

THIS PAGE IS UNCLASSIFIED

AD837231

SEISMIC DATA LABORATORY
QUARTERLY TECHNICAL SUMMARY REPORT

APRIL - JUNE 1968

15 JULY 1968

Prepared For

AIR FORCE TECHNICAL APPLICATIONS CENTER
Washington, D. C.

By

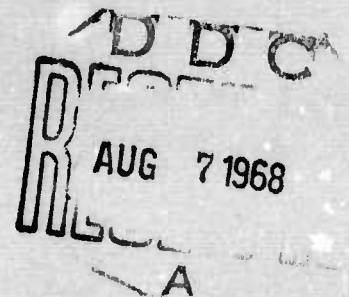
TELEDYNE, INC.

Under

Project VELA UNIFORM

Sponsored By

ADVANCED RESEARCH PROJECTS AGENCY
Nuclear Test Detection Office
ARPA Order No. 624



SEISMIC DATA LABORATORY
QUARTERLY TECHNICAL SUMMARY REPORT
April - June 1968

15 July 1968

AFTAC Project No.:	VELA T/6702
Project Title:	Seismic Data Laboratory
ARPA Order No.:	624
ARPA Program Code No.:	8F10
Name of Contractor:	TELEDYNE INDUSTRIES, INC.
Contract No.:	F33657-68-c-0945
Date of Contract:	2 March 1968
Amount of Contract:	\$1,251,000
Contract Expiration Date:	1 March 1969
Project Manager:	Royal A. Hartenberger (703) 836-7647

P.O. Box 334, Alexandria, Virginia

AVAILABILITY

This document is subject to special export controls and each transmittal to foreign governments or foreign nationals may be made only with prior approval of Chief, AFTAC.

attn: VSC

9/12/68 70333

SEISMIC DATA LABORATORY
QUARTERLY TECHNICAL SUMMARY REPORT
April - June 1968

15 July 1968

AFTAC Project No.:	VELA T/6702
Project Title:	Seismic Data Laboratory
ARPA Order No.:	624
ARPA Program Code No.:	8F10
Name of Contractor:	TELEDYNE INDUSTRIES, INC.
Contract No.:	F33657-68-c-0945
Date of Contract:	2 March 1968
Amount of Contract:	\$1,251,000
Contract Expiration Date:	1 March 1969
Project Manager:	Royal A. Hartenberger (703) 836-7647

P.O. Box 334, Alexandria, Virginia

AVAILABILITY

This document is subject to special export controls and each transmittal to foreign governments or foreign nationals may be made only with prior approval of Chief, AFTAC.

The work reported herein was supported by the Advanced Research Projects Agency, Nuclear Test Detection Office, under Project VELA-UNIFORM and accomplished under the technical direction of the Air Force Technical Applications Center under Contract F33657-68-c-0945.

Neither the Advanced Research Projects Agency nor the Air Force Technical Applications Center will be responsible for information contained herein which may have been supplied by other organizations or contractors, and this document is subject to later revision as may be necessary.

TABLE OF CONTENTS

	<u>Page No.</u>
ABSTRACT	
I. INTRODUCTION	1
II. WORK COMPLETED	1
A. Precision Location of Underground Nuclear Explosions Using Teleseismic Networks and Pre-determined Travel-Time Anomalies	1
B. Preliminary Beamforming Study of the TFO-37 Array	8
C. P Wave Parameters Measured at the Montana LASA	11
D. An Analysis of a Technique for the Generation of High Resolution Wavenumber Spectra.	21
E. Vertical Array Frequency-Wavenumber (v-f-k) Spectra of Synthesized Rayleigh Wave and P-Wave Noise.	25
F. Earthquake and Explosion Analysis	29
III. SUPPORT AND SERVICE TASKS	29
A. VELA-Uniform Data Services	29
B. Data Library	30
C. Data Compression	33
D. Automated Bulletin Process	33
APPENDIX A - Organizations Receiving SDL Data Services	

LIST OF FIGURES

Figure No.	Follows Page
1. Nevada Test Site Area	2
2. Maximum-relative-error output from SIGRID; event Bourbon	4
3. Standard-deviation output from SIGRID; event Bourbon	4
4. Bandpass filters used in data preparation	9
5. Earthquake, South Pacific, 24 February 1968, phased sum	9
6. Power spectra of unfiltered noise Hokkaido, 25 Feb. 1968	10
7. Noise power spectra, Hokkaido, 25 February 1968	10
8. Noise power spectra, South Pacific, 24 February 1968	10
9. Noise Power spectra, Peru, 24 February 1968	10
10. Noise power spectra, Tunisia, 25 February 1968	10
11. Observed azimuth deviations for events with epicenters located along the northwest profile, 300°-320°	13
12. Observed values of p for events with epicenters located along the northwest profile, 300°-320°	13
13. p versus distance curves	14
14. Observed azimuth deviations for events with epicenters located along the southeast profile, 140°-160°	16
15. Observed values of p for events with epicenters located along the southeast profile, 140°-160°	17
16. p versus distance curves	17
17. WMSO surface array	21
18. The WMO array response to an infinite-velocity plane wave	21
19. The ordinary f-k spectrum of a theoretical 12.0 km/sec plane wave arriving at WMO from the south; the frequency is 0.3125 cps.	22
20. The high-resolution f-k spectrum of the 12.0 km/sec event at 0.3125; S/N = .03.	22

LIST OF FIGURES

Figure No.	Follows Page
21. The high-resolution f-k spectrum for the 12.0 km/sec plane waves at frequency at 0.3125 cps. The reference seismometer is located at (.94,-.17); S/N = .03	22
22. The high-resolution f-k spectrum for the 12 km/sec plane wave at .3125 cps averaged over all of the seismometers; S/N = .03	22
23. Ordinary f-k spectrum of LONG SHOT at LASA subarray F1 at .625 cps.	23
24. High-resolution f-k spectrum of LONG SHOT at LASA F1, averaged over all seismometers in the array at .625 cps. C=2.0	23
25. Beam-steered power-density spectrum of the LONG SHOT event at LASA F1	23
26. Array response of the partial XE3 array to an infinite velocity plane wave	23
27. Ordinary f-k spectrum at .625 cps of two plane waves, one of amplitude 1 at 20 km/sec, North; and one of amplitude .2 at 30 km/sec, South	23
28. High-resolution wavenumber-spectrum of the two plane waves at .625 cps averaged over all of the sensor in the array S/N = 2.0	23
29. High-resolution wavenumber spectrum of the two plane waves at .625 cps averaged over all of the sensors in the array. S/N = .03	24
30. Frequency-Amplitude-Depth Relations for fundamental Rayleigh mode at station APOK	26
31. Frequency-Amplitude-Depth relations for higher Rayleigh modes at station APOK first higher mode	26
32. Frequency-Amplitude-Depth relations for higher Rayleigh modes at station APOK second higher mode	26
33. Frequency-Amplitude-Depth relations for higher Rayleigh modes at station APOK third higher mode	26
34. Velocity and density sections at site APOK (Apache, Oklahoma)	26

LIST OF FIGURES

Figure No.	Follows Page
35. Fundamental Rayleigh mode - vertical component station APOK	27
36. 1st higher Rayleigh mode - vertical component station APOK	27
37. 2nd higher Rayleigh mode - vertical component station APOK	27
38. 3rd higher Rayleigh mode - vertical component station APOK	27
39. Teleseismic P-wave noise - vertical component station APOK	28
40. Teleseismic P-wave signal (white)-vertical component station APOK	28

LIST OF TABLES

TABLE TITLE	TABLE NO.
Event Information	I
Station Anomalies and Residuals	II
Arrival Time Data	III
Location Errors when Neither Residuals nor Anomalies are Used	IV
Location Errors when Residuals or Anomalies are Used	V
Confidence Regions SHIFT-61	VI
TFC-37 amplitudes for data prefiltered 0.4 - 3 and 0.7-5 cps	VII
LASA Bulletin Statistics for Four Teleseismic Events	VIII
Seismic Data from Two Nuclear Explosions	IX

ABSTRACT

This report summarizes the work done by the SDL during the period April through June 1968, and is primarily concerned with seismic research activities related to the detection and identification of nuclear explosions and earthquake phenomenon. Also discussed are the support tasks and data services performed for other participants in the VELA-Uniform project.

I. INTRODUCTION

This quarterly report summarizes the technical work, support effort, and service tasks completed during the period April through June 1968. Current or past work is mentioned only if it relates to the present discussions.

Reviews of technical reports completed during the reporting period are contained in Section II under descriptive headings. Section III is a summary of the support and service tasks performed for in-house projects and for other VELA-Uniform participants. This report concludes with Appendix A in which are listed the organizations who received SDL data services during the period.

II. WORK COMPLETED

A. Precision Location of Underground Nuclear Explosions Using Teleseismic Networks and Predetermined Travel-Time Anomalies

This report is primarily concerned with the teleseismic location accuracy obtainable for a particular region by using either station residuals, travel-time anomalies, or no corrections at all. Secondly, we are concerned with the performance of two computer programs, LOCATE and SHIFT, presently in use at the Seismic Data Laboratory. The principal difference between the two programs is that SHIFT minimizes in a least-squares sense the relative-anomaly errors rather than the absolute residuals.

Also investigated is a technique whereby limits of the solution are estimated either on the basis of an acceptable network standard deviation of time errors or of maximum relative-time errors at any station pair within the network.

All of the time data used in this study were derived from nuclear explosions detonated within the Nevada Test Site (NTS) area (Figure 1). Table I lists the event information. The events selected as references from which residuals and anomalies were measured are Bilby or Tan, the series of Bronze, Corduroy, and Buff, or the series of Nash, Agile, and Commodore. These several events were necessary so that residuals or anomalies could be obtained for an adequate number of recording stations. Table II lists the station anomalies, relative to RK-ON, computed from the travel-time tables, in addition to the residuals computed from the Herrin/1961 table. A key letter, indicating which series of events were used as references in determining the corrections is given in the last column.

Station records of all explosions were routinely read, with the identical networks of stations and arrival times being used for both programs. Depths for all events were restrained to the surface. Raw arrival times (Table III) were input to SHIFT and used within the program in conjunction with the appropriate input travel-time anomalies. For LOCATE, station arrival times were corrected by the residuals prior to their input into the program. These input times for LOCATE are obtained by subtracting the residuals in Table II from the arrival times input to SHIFT (Table III).

A description of the use of program SHIFT is given in Appendix I of the original report.

Without Time Corrections - Table IV lists the location errors, in kilometers, when neither residuals nor anomalies are applied to the event arrival times (the times have been corrected, however, for station elevation and ellipticity). The mean error

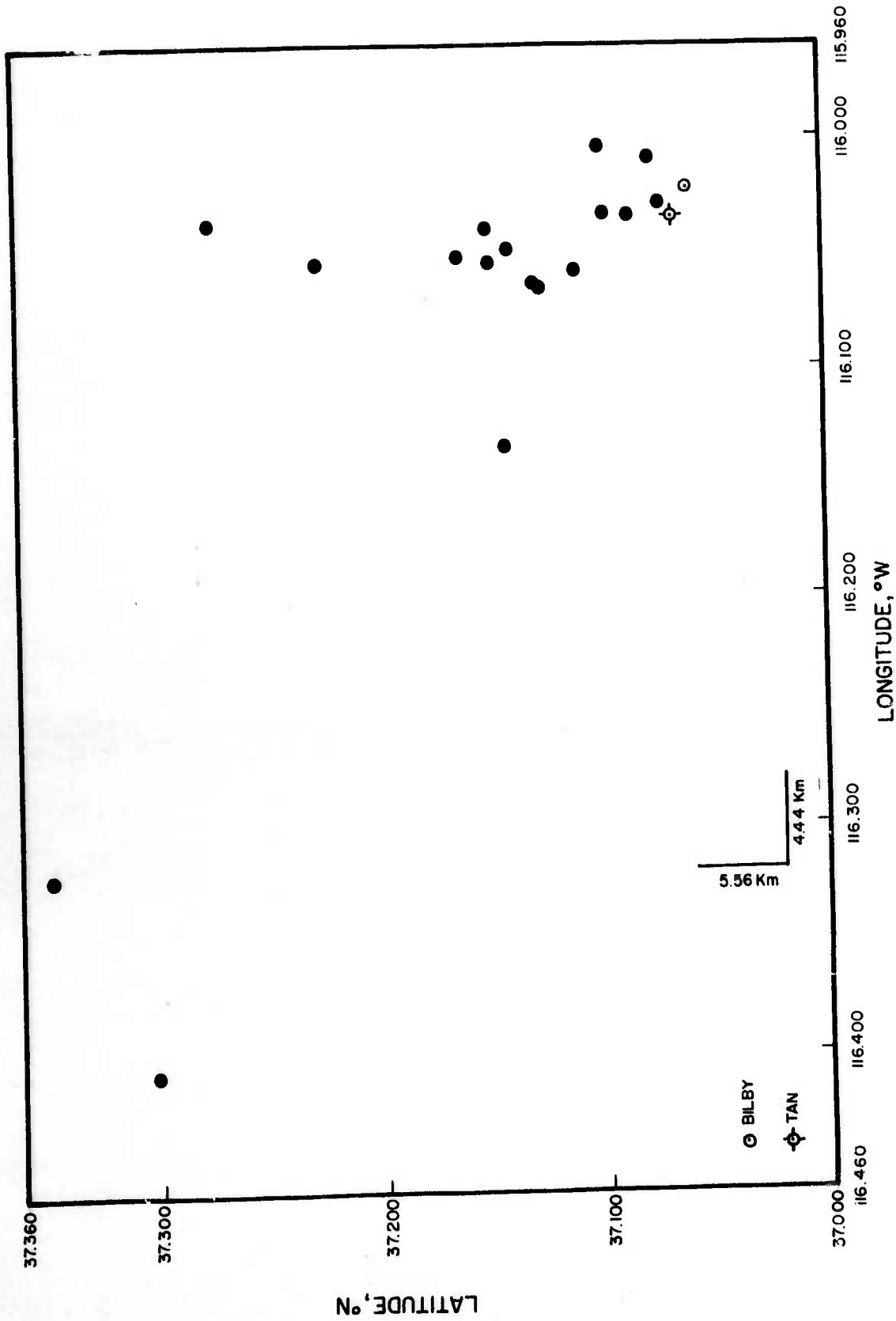


Figure 1. Nevada Test Site Area

TABLE I
Event Information

<u>Event</u>	<u>Date</u>	<u>Origin Time</u>	<u>Latitude</u>	<u>Longitude</u>	<u>No. of Stations</u>
AUK	02 Oct 64	20 03 00.0	37.078N	116.009W	6
FORE	16 Jan 64	16 00 00.1	.142	.049	12
DUMONT	19 May 66	13 56 28.1	.111	.058	8
CHARTREUSE	06 May 66	15 00 00.1	.348	.322	7
TURF	24 Apr 64	20 10 00.2	.150	.055	10
KLICKITAT	20 Feb 64	15 30 00.1	.151	.040	9
PILEDRIVER	02 Jun 66	15 30 00.1	.227	.055	7
BRONZE	23 Jul 65	17 00 00.0	.098	.033	9
CORDUROY	03 Dec 65	15 13 02.1	.165	.052	9
BUFF	16 Dec 65	19 15 00.0	.073	.029	8
GREELEY	20 Dec 66	15 30 00.1	.302	.408	13
PIRANHA	13 May 66	13 30 00.0	.087	.034	9
NASH	19 Jan 67	16 45 00.1	.144	.136	7
BOURBON	20 Jan 67	17 40 04.1	.100	.004	4
AGILE	23 Feb 67	18 50 00.0	.127	.067	7
COMMODORE	20 May 67	15 00 00.2	.130	.064	5
SCOTCH	23 May 67	14 00 00.0	.275	.370	5
BILBY	13 Sep 63	17 00 00.1	.061	.022	14
TAN	03 Jan 66	14 00 00.0	.068	.035	8

TABLE II
Station Anomalies and Residuals

<u>Station</u>	<u>Anomaly Relative to RK-ON</u>			<u>Residual Herrin 61</u>	<u>Event Key*</u>
	<u>Herrin 61</u>	<u>Herrin 66</u>	<u>JB</u>		
AD-IS	+1.11 sec	+0.04 sec	+0.57 sec	-1.1 sec	B
AX2AL	+2.21	+1.61	+2.23	+0.2	A
BE-FL	+1.11	+1.11	+1.15	-0.9	A
BL-WV	+0.66	+0.61	+0.84	-1.6	A
BR-PA	+0.74	+0.76	+0.84	-1.5	A
CPO08	+1.51	+0.86	+1.55	-0.6	A
DH-NY	+0.09	+0.03	+0.11	-2.2	A
EB-MT	-0.84	+0.08	-0.68	-3.1	A
EN-MO	+0.08	+0.54	+0.04	-2.0	B
EU-AL	+2.66	+1.94	+2.71	+0.6	A
GG-GR	+1.06	+1.00	+2.07	-1.2	A
HN-ME	+1.11	+0.55	+0.97	-1.0	A
KC-MO	+1.71	+1.81	+1.45	-0.7	D
LV-LA	+1.51	+1.90	+1.48	-0.6	A
LZ-BV	+0.90	+0.94	+1.19	-1.9	A
NP-NT	+1.88	+0.96	+1.52	-0.2	A
OO-NW	-0.01	+0.01	+0.52	-2.4	A
PG-BC	+2.66	+2.94	+2.57	+0.3	C
PZ-PR	+2.28	+1.17	+1.53	+0.1	A
SI-BC	+1.87	+2.81	+2.05	-0.2	A
SV2QB	+0.35	-0.37	+0.16	-2.0	A**
SV3QB	+0.35	-0.37	+0.16	-2.0	A
WH2YK	+1.36	+1.13	+1.50	-0.8	C
RK-ON	0	0	0	-2.1	A

*A = Bilby-Tan
 B = Bronze-Corduroy-Buff
 C = Nash-Agile-Commodore
 D = Greeley

**Set equal to anomaly for SV3QB determined from A

TABLE III - Arrival Time Data

Event Reference Hour	Bilby 17	Tan 14	Auk 20	Fore 16	Dumont 14	Chartreuse 15	Turf 20	Klickitat 15	Piledriver 15	Bronze 17
<u>STATION</u>										
AD-IS										0812.2
AX2AL		0525.4			0153.6	0527.7			3525.5	
BE-FL		0607.2			0235.6		1548.9		3607.7	0548.4
BL-WV	0548.4			0548.9				3548.6		
BR-PA	0603.0			0603.3			1603.4	3603.1		0603.1
CPO	0521.6	0521.7	0821.9	0521.7	0149.9	0523.7	1522.1	3521.8	3521.8	0521.7
DH-NY	0626.7		0926.8				1627.3	3626.7		0626.7
EB-MT	0426.8			0426.4			1426.6	3426.5		
EN-MO										
EU-AL	0512.2			0512.6						
GG-GR	1221.9			1221.0			2222.7	4221.2		
HN-ME	0707.9	0708.1	1007.9	0707.8	0336.1	0708.8	1707.9	3707.9	3707.5	0707.9
KC-MO										
LV-LA	0441.1			0441.6						
LZ-BV	1111.0		1411.10				2111.6			
NP-NI	0731.5	0731.1	1031.3	0730.8	0358.7	0729.0	1730.6	3730.6	3729.9	0730.8
OO-NW	1131.8			1131.5						
PG-BC										
P2-PR	0837.0			0838.1						
SI-BC		0428.5		0055.9		0424.4			3426.7	
SV2QB										0716.0
SV3QB		0716.5		0344.3		0715.2				
WH2YK										
RK-ON	0445.8	0445.9	0745.8	0445.4	0113.6	0445.2	1445.4	3445.1	3444.7	0445.5
	13	7	6	11	7	6	9	8	6	8

TABLE III (Continued)

Hour Reference	Hour 15	Corduoy 15	Buff 19	Greeley 15	Bourbon 17	Agile 18	Nash 16	Commodore 15	Piranha 13	Scotch 14
STATION										
AD-IS	2113.9	2312.5								
AX2AL		3528.1							3525.7	
BE-FL	1909.5	3610.0							3607.6	
BL-WV										
BR-PA										
CPC	1823.8	2021.8	3524.2		5522.0	5022.7			3521.9	
DH-NY										
EB-MT										
EN-MO	1740.2	1938.0								
EU-AL		3515.0								
GG-GR		4221.2								
HN-ME	2009.6	2207.8	3709.0		4711.4	5708.1	5208.8	0708.1	3708.3	0709.2
KC-MO		3401.7								
LV-LA										
LZ-BV										
NP-NT	2032.5	2231.2	3728.2		4734.6	5730.8	5231.0		3731.3	
OO-NW		4130.7								
PG-BC		3403.6				5406.5	4906.7	0406.4	3407.5	0404.3
PZ-PR										
SI-BC	1729.5	1928.4							3428.4	
SV2QB										
SV3QB	2018.0	2216.5	3716.3		4719.9	5716.5	5216.7	0716.3	3716.5	0716.5
WH2YK		3536.8				5539.8	5039.4	0539.4		0537.7
RK-ON	1747.1	1945.7	3445.8		4449.1	5445.7	4946.2	0445.7	3445.8	0446.0
	8	7	12		3	6	6	4	6	4

TABLE IV

Location Errors when Neither Residuals
nor Anomalies are Used

<u>EVENT</u>	<u>NO. OF STATIONS</u>	<u>LOCATE-H61</u>	<u>SHIFT-H61</u>	<u>SHIFT-H66</u>	<u>SHIFT-JB</u>
Buff	8	9.1	8.6	10.9	5.7
Turf	10	14.5	15.0	8.0	18.3
Corduroy	9	11.6	10.8	5.2	6.3
Nash	7	17.2	18.1	13.4	23.1
Bourbon	4	48.0	49.0	17.6	42.6
Piledriver	7	39.6	39.3	37.7	41.9
Bronze	9	13.3	13.1	8.5	12.3
Auk	6	7.1	7.2	3.7	4.8
Piranha	9	41.1	40.4	45.5	46.3
Fore	12	38.1	38.5	20.0	36.6
Greeley	13	10.1	12.3	11.6	25.5
Dumont	8	43.0	43.6	44.9	47.1
Chartreuse	7	60.0	59.8	48.5	62.8
Commodore	5	11.1	10.9	23.3	12.6
Agile	7	23.4	23.0	15.0	27.7
Scotch	5	17.4	17.8	26.6	19.6
Klickitat	9	33.5	33.7	12.8	38.2
∑		438.1	441.1	353.2	471.4
Mean error, km		25.8	25.9	20.8	27.7

for 17 events using LOCATE is seen to be 25.8 km and using SHIFT (Herrin 61) 25.9 km/ the results from the two programs using the same travel-time table are essentially in agreement. With the J-B and Herrin 66 tables, the results using SHIFT are 27.7 km and 20.8 km respectively. It is not known at this time if the apparently better results obtained by using the Herrin 66 table are significant or not. It would be necessary to locate a larger sample of events to determine the effectiveness of this table for the networks used in this study and for the NTS area.

The resultant average errors of about 26 km demonstrate the best one could hope to do when no allowances are made for residuals (LOCATE) or anomalies (SHIFT).

With Time Corrections - When the residuals or anomalies are determined for a particular region, such as the Nevada Test Site, and for each station which is to be used in subsequent location networks, the resultant location errors can be reduced by at least an order of magnitude. Table V lists the location errors, in kilometers, when either residuals (LOCATE) or relative anomalies (SHIFT) are applied to the event arrival times. The mean error for 17 events using LOCATE is now seen to be 2.98 km and using SHIFT (Herrin 61) 2.86 km. Again, the mean values from either program are in agreement, although individual event locations differ by as much as 4.1 km between the two methods. This difference implies, of course, that the programs are computing in significantly different ways but yield about the same answer on the average. Using the J-B and Herrin 66 tables, the SHIFT mean errors are 2.92 km and 2.59 km, respectively, which suggests that when anomalies are applied, any reasonable travel-time table is adequate.

TABLE V
Location Errors When Residuals
or Anomalies are Used

<u>EVENT</u>	<u>NO. OF STATIONS</u>	<u>LOCATE-H61</u>	<u>SHIFT-H61</u>	<u>SHIFT-H66</u>	<u>SHIFT-JB</u>
Buff	8	2.4	0.1	0.3	0.2
Turf	10	0.5	0.1	0.2	0.1
Corduroy	9	1.6	1.0	0.9	0.9
Nash	7	5.8	1.7	1.4	1.8
Bourbon	4	2.8	1.9	2.1	1.9
Piledriver	7	2.0	2.9	1.5	3.3
Bronze	9	4.2	3.0	2.7	2.9
Auk	6	3.1	3.0	2.9	3.0
Piranha	9	0.8	3.1	2.7	3.2
Fore	12	3.3	3.2	2.9	3.1
Greeley	13	1.0	3.3	3.8	3.3
Dumont	8	2.2	3.4	3.0	3.4
Chartreuse	7	5.7	3.6	3.7	4.2
Commodore	5	4.1	3.7	3.2	3.3
Agile	7	1.5	3.9	2.4	3.1
Scotch	5	3.6	5.0	4.8	5.7
Klickitat	9	6.1	6.0	5.6	6.2
∑		50.7	48.9	44.1	49.6
Mean error, km		2.98	2.86	2.59	2.92

Confidence regions were computed within SHIFT in the usual manner (e.g., Flinn, 1965) for all events, both with and without travel-time anomalies. Table VI lists, by event, the areas of the computed ellipses and the factors of reduction in ellipse areas when anomalies are used. Without anomalies, two events (Fore and Chartreuse) were not within the ellipse at the 95% level. With anomalies, all events were within the ellipse and the ellipses were reduced in area by factors of 5 to 152, with an average reduction of about 45. This reduction in ellipse area points out the necessity and value of travel-time anomalies.

The dashed-line polygon in Figure 2 is the contour of the (known) maximum relative error (0.18 sec) at the true epicenter marked at X. The circle enclosing the value 0.11 is the maximum relative error as a result of the final solution obtained with SHIFT-H61. The solid-line polygon is the contour of the maximum relative error estimated to be 0.4 sec (0.3 sec higher than that at the final solution) for this event. A seismic analyst can usually estimate his reading errors quite well, and if the effects of previously determined relative travel-time anomalies are removed (they must be determined, not estimated); the estimates can be used to contour the maximum relative error. A relative error estimate of 0.4 sec is liberal for an event of the size of Bourbon, but it is an example of the manner of using any estimate. The approximate area of the estimated polygon is less than 340 km^2 . The area of the corresponding ellipse previously computed (Table VI) is 7118 km^2 .

Subroutine SIGRID produces an output of network standard deviations, in addition to the maximum relative errors, for a similar set of grid positions. Figure 3 shows the zero-mean standard deviation output for Bourbon, with anomalies.

TABLE VI

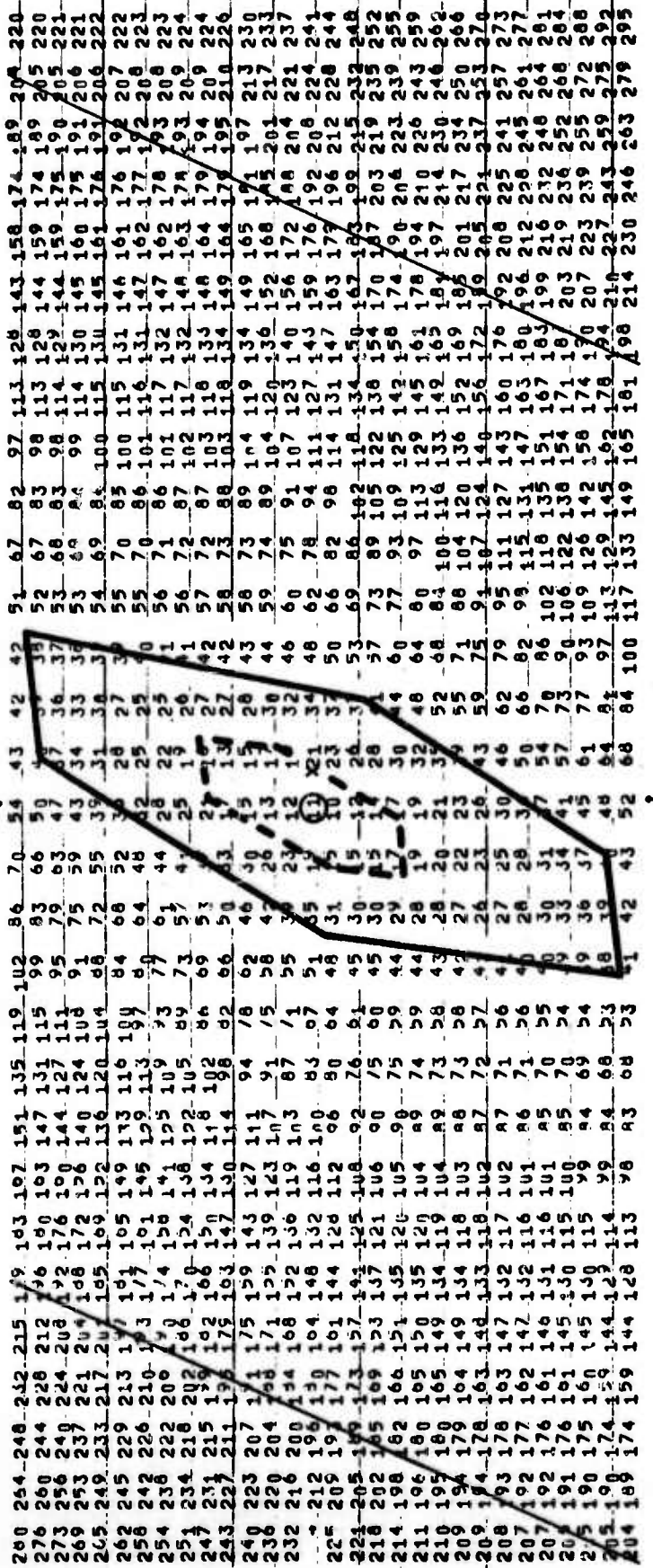
Confidence Regions
SHIFT-61

Event	Ellipse Areas km ²		Improvement Factor, a/b	No. of Stations
	Without anomalies a	With anomalies b		
Fore	2059*	348	6	12
Buff	2402	50	48	8
Chartreuse	1041*	131	8	7
Auk	10035	66	152	6
Bourbon	206088	7118	29	4
Dumont	1495	52	29	8
Agile	4020	234	17	7
Nash	7256	113	64	7
Commodore	27698	288	96	5
Greeley	2620	96	27	13
Klickitat	2384	202	12	9
Turf	2513	524	5	10
Piranha	2159	15	144	9
Scotch	37869	2309	16	5
Corduroy	1564	25	62	9
Bronze	2038	25	81	9
Piledriver	1593	79	20	7

*Confidence ellipse does not contain true epicenter.

20 JAN 67 BOURBON

MAXIMUM RELATIVE ERROR • 100.



HERRING61 TRAVEL TIME TABLES

02 07 68 20 JAN67 BOURBON

REFERENCE LATITUDE 37.0997 ON LINE 15
 LONGITUDE 115.6228 IN COLUMN 15
 DEPT 0

UPPER LEFT 37.2259 LOWER LEFT 36.9648
 LONGITUDE 115.6199 LONGITUDE 115.6199
 INCREMENT DEG ARC KM UPPER RIGHT 37.2256 LOWER RIGHT 36.9648
 .0090 1.00 .0271 2.48

STANDARD DEVIATION OF ERRORS = 1.00

123	115	108	100	93	85	78	71	63	56	49	42	35	29	24	19	17	19	23	28	34	41	48	55	62	70	77	84	92	99
121	114	106	99	92	84	77	69	62	55	48	41	34	28	22	18	16	18	23	28	35	42	49	56	63	70	78	85	93	100
120	113	105	98	90	83	75	68	61	53	46	39	32	26	20	16	15	18	23	29	35	42	49	57	64	71	79	86	94	101
119	111	104	96	89	82	74	67	59	52	45	38	31	24	19	15	14	17	23	29	36	43	50	57	65	72	80	87	95	102
118	110	103	95	88	80	73	65	58	51	43	36	29	23	17	13	13	17	23	29	36	44	51	58	66	73	81	88	96	103
116	109	101	94	86	79	71	64	57	49	42	35	28	21	16	12	13	17	23	30	37	44	52	59	67	74	81	89	96	104
115	108	100	93	85	78	70	63	55	48	41	33	26	20	14	11	12	17	24	31	38	45	53	60	67	75	82	90	97	105
114	106	99	91	84	76	69	61	54	47	39	32	25	18	12	10	12	18	24	31	39	46	53	61	68	76	83	91	98	106
113	105	98	90	83	75	68	60	53	45	38	31	23	17	11	9	12	18	25	32	40	47	54	62	69	77	84	92	99	107
111	104	96	89	81	74	66	59	51	44	37	29	22	15	9	7	12	19	26	33	40	48	55	63	70	78	85	93	100	108
110	103	95	88	80	73	65	58	50	43	35	28	21	14	8	7	13	19	27	34	41	49	56	64	71	79	86	94	102	109
109	102	94	87	79	72	64	57	49	42	34	27	19	12	7	7	13	20	27	35	42	50	57	62	72	80	87	95	103	110
108	100	93	85	78	70	63	55	48	40	33	25	18	11	6	7	14	21	28	36	43	51	58	66	73	81	89	96	104	111
107	99	92	84	77	69	62	54	47	39	32	24	17	10	5	5	15	22	29	37	44	52	59	67	75	82	90	97	105	112
105	97	89	82	74	67	59	52	44	37	29	22	15	8	5	10	17	24	32	39	47	54	62	69	77	84	92	99	107	115
103	96	88	81	73	66	58	51	43	36	28	21	14	7	6	11	18	25	33	40	48	55	63	70	78	85	93	101	108	116
102	95	87	80	72	65	57	50	42	35	27	20	13	7	7	12	19	27	34	42	49	57	64	72	79	87	94	102	109	117
101	94	86	79	71	64	56	49	41	34	27	19	13	7	7	14	21	28	35	43	50	58	65	73	80	88	95	103	110	118
100	93	85	78	70	63	55	48	40	33	26	19	12	6	9	15	22	29	37	44	51	59	66	74	81	89	97	104	112	119
99	92	84	77	69	62	54	47	39	32	25	18	12	9	11	17	23	31	38	45	53	60	68	75	83	90	98	105	113	120
98	91	83	76	68	61	53	46	39	31	24	18	12	10	12	18	25	32	39	47	54	61	69	76	84	91	99	106	114	122
97	90	82	75	67	60	52	45	38	31	24	17	12	11	14	20	26	33	41	48	55	63	70	78	85	93	100	108	115	123
96	89	81	74	66	59	52	44	37	30	23	17	13	12	16	21	28	35	42	49	57	64	71	79	86	94	101	109	116	124
95	88	80	73	65	58	51	44	36	29	23	17	13	13	17	23	29	36	43	51	58	65	73	80	88	95	103	110	118	125
94	87	79	72	65	57	50	43	36	29	23	17	14	15	19	24	31	38	45	52	59	67	74	81	89	96	104	111	119	126
93	86	78	71	64	56	49	42	35	29	23	18	15	16	20	26	32	39	46	53	61	68	75	83	90	98	105	113	120	128
92	85	78	70	63	56	49	42	35	28	23	18	16	18	22	27	34	41	48	55	62	69	77	84	91	99	106	114	121	129
91	84	77	69	62	55	48	41	34	28	23	19	17	19	23	29	35	42	49	56	63	71	78	85	93	100	108	115	123	130
90	83	76	69	61	54	47	40	34	28	23	19	19	21	25	31	37	44	51	58	65	72	79	87	94	102	109	116	124	131

○ Final location from SHIFT-H61
 X Actual epicenter of Bourbon
 ---Contour of actual standard deviation

Figure 3. Standard-deviation output from SIGRID; event Bourbon

The following conclusions are made concerning the results obtained by analyzing 19 nuclear explosions detonated within a 2500 km² area of the Nevada Test Site. Seismograms were used from teleseismic stations forming networks of four to thirteen stations.

1. For limited-station teleseismic networks, the location capability for 17 events occurring in the Nevada Test Site and without applying previously-determined residuals or travel-time anomalies, is about 26 km, regardless of the program used (LOCATE or SHIFT) and regardless of the travel-time table employed (Herrin 61, Herrin 66, or J-B tables).

2. The location capability for the same networks and time data is better than 3 km when previously-determined residuals or travel-time anomalies are applied, regardless of program and travel-time table. That is to say, when these travel-time curves can equivalently be replaced by observed travel times from each station to an accurately known explosion point, the particular curve selected as a standard is essentially irrelevant and epicenters of other nearby explosions can be located within the indicated error limit.

3. The effect of the number of stations in the range from 3 or 4 to 13 on the location capability of the networks used in the study is negligible, either with or without travel-time anomalies.

4. The effect of the range of epicentral distances (distance aperture) on the capability of locating known surface events with the same networks is negligible, either with or without travel-time anomalies.

5. The azimuth aperture has an observable effect on the location capability of the networks where, for apertures down to 60° , the location errors without travel-time anomalies are as high as 60 km, and with anomalies 6 km.

6. The areas of computed confidence ellipses can be reduced by factors of 1/5 to 1/152 with the application of travel-time anomalies and still enclose the event locations which, for this study, are accurately known, as are the explosions used to calibrate the particular epicenter-station paths used in the study. In effect, these reduced ellipses represent uncertainties in the position of the epicenters relative to the position of the calibration events.

7. With as few as 4 or 5 stations, computed confidence ellipses with anomalies are unrealistically large due to the small number of statistical degrees of freedom. (The Bourbon explosion, with 4 stations, has an ellipse $7,000 \text{ km}^2$ and a location error of 1.9 km). Estimates of the maximum relative time errors for a network of stations permits more realistic confidence limits to be set on the solution. In this way, Bourbon's confidence polygon is about 340 km^2 . Also, as few as three stations can be used to obtain the confidence limits when maximum relative errors are estimated.

8. Travel-time anomalies, computed from a few selected events, show some variability across the NTS area in Figure 1, but the effect on relative location accuracy is small. The size of the area in Figure 1 is about 2500 km^2 , implying that fairly large regions are involved for determining reasonably constant anomalies, so the problem of time calibrating a stationary network for any region of the earth from which either explosions

at accurately known locations or earthquakes (bias effects not included) are recorded is not formidable. In either case, if accurate locations are not independently known, the epicentral solutions with anomalies included reduce to locations relative to one another with the actual error of the whole set remaining unknown.

9. Relative anomalies for earthquake regions can be simpler to assess than absolute residuals because (a) origin time errors are eliminated; (b) first-extremum anomalies and first motion anomalies from several events can be combined (except when obvious period differences are noted); and (c) depending on the region and on the network geometry, the regions for which the calibrations need to be determined can be fewer in number and larger in area.

References

Chiburis, E.F., and Dean, W.C., 1965, Teleseismic Signal Alignment at the Tonto Forest Extended Array; Teledyne Report No. 125, 15 October.

Chiburis, E.F., 1966a, Relative Travel-Time Anomalies at LASA and the Location of Epicenters using SHIFT; Teledyne Report No. 147, 7 June.

Chiburis, E.F., 1966b, LASA Travel-Time Anomalies for Various Epicentral Regions; Teledyne Report No. 159, 13 September.

Chiburis, E.F., 1968, LASA Travel-Time Anomalies for 65 Regions Computed with the Herrin Travel-Time Table, November 1966 Version; Teledyne Report No. 204, 10 January 1968.

Flinn, E.A., 1965, Confidence Regions and Error Determinations for Seismic Event Location; Reviews of Geophysics, Vol. 3, No. 1.

B. Preliminary Beamforming Study of the TFO-37 Array

This study describes a preliminary evaluation of the new TFO array in terms of the amount of signal loss, noise attenuation, and S/N gain which result from beamforming digital recordings of four teleseismic events. The array consists of 37 JM short-period vertical seismometers arranged to form three concentric hexagons containing six, twelve, and eighteen sensors, respectively, with an additional sensor in the center. The approximate diameter of the outside hexagon is thirty kilometers, and intersensor spacing is approximately five kilometers.

In addition to presenting the results of a basic investigation, another intention is to assemble information pertaining to the array in one report which can serve as a reference for future studies. With this in mind, the following appendices are included in the original report:

Appendix A: Map of Array

Appendix B: Seismometer description and locations in latitude and longitude

Appendix C: Digital tape format

Appendix D: Digital programs written for the evaluation

Appendix E: Calibration parameters

Appendix F: Sample output from which Table VII was prepared

Appendix G: JM frequency response

The LASA Bulletin statistics for the data are shown in Table VIII. Since this report includes only a small number of events, one from each quadrant was selected to give full azimuthal coverage.

Table VIII. LASA bulletin statistics for four teleseismic events

DATE	EVENT NAME	MAG	LAT	LONG	ORIGIN TIME	TFO TAPE NO.
25 FEB 68	HOKKAIDO	5.4	44.5 N	141.7 E	10:25:43.0	378
24 FEB 68	SO. PACIFIC	5.1	35.0 S	169.8 W	01:11:27.0	364
24 FEB 68	PERU	5.0	16.3 S	71.7 W	07:31:28.0	367
25 FEB 68	TUNISIA	4.8	36.0 N	10.8 E	15:40:28.0	380

Table VII summarizes the final results of the amplitude analysis and contains three major headings, Signal, Noise, and S/N. As shown in Table VII, there is a slight loss in signal amplitude between the mean and the sum possibly due to small misalignments. In addition, the apparent db loss also can be attributed to the signal/noise ratio. The Tunisia earthquake is poorly recorded and the "P" probably contains some noise which precludes an accurate estimate of signal amplitude during the phasing process. A deterioration in amplitude (μ) is obvious between the SDL and Fc filter (Figure 4) amounting to about 4 db in all cases. This suggests that the SDL filter is more effective in preserving signal amplitude within the frequency range of the events studied. On the other hand, an examination of Figure 5 reveals the undesirable loss of first motion as well as a loss of signal character caused by the SDL filter which appears to over-simplify the signature.

With respect to the noise, both prefilters yield an acceptable reduction in rms, but the Fc is the better of the two. This is due to the removal of the low frequency microseisms which predominate. The amplitude of the maximum noise excursion, indicated by the heading RANGE, is also shown. The ratio of the Range/rms is approximately 3/1, a value normally considered when referring to peak versus average rms noise.

The last heading in the table concerns S/N ratio. Again, both filters function well but the Fc responds best by about 3 db over the SDL.

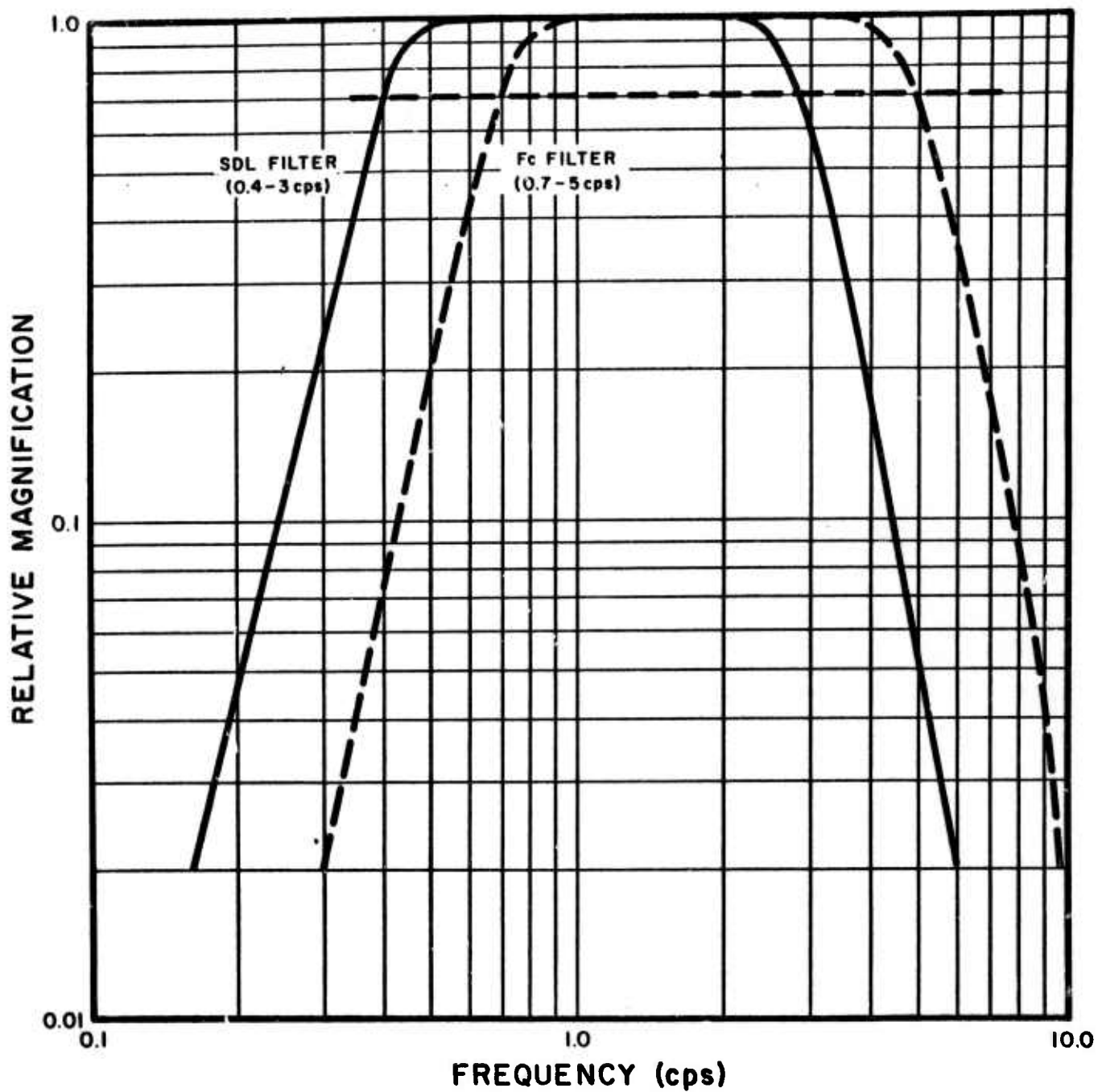


Figure 4. Bandpass filters used in data preparation.

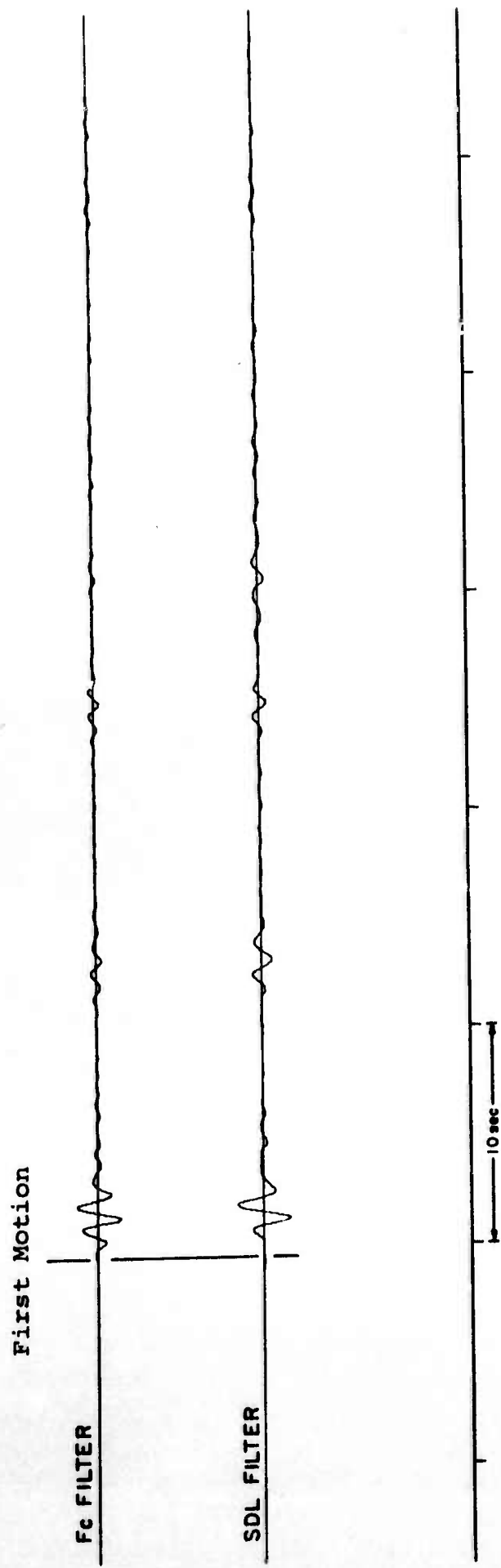


Figure 5. Earthquake, South Pacific, 24 February 1968, phased sum.

Power spectra were completed for the 100 seconds of noise preceding each of the four events by a digital program based on the Blackman and Tukey method. Figures 7 through 10 each illustrate the results of spectral analysis of noise occurring prior to the signal on the phased sum and the average noise spectra of outputs recorded by 18 to 19 individual elements. It was felt that taking the average of a number of sensors was better than selecting just one, and that spatial sampling of the array would give about the same results as processing the total.

The spectral shape is approximately the same for any given filter and will not vary much whether the analysis is performed on an individual trace or the phased sum of many. In all examples shown, summing the elements attenuates the noise at, for example, 1 cps approximately 15 db over the average single instrument which is equal to a factor of N . The best S/N ratio, again referring to Table VII, is several db lower. For comparative purposes, Figure 6 shows the results of raw data processing of the Hokkaido event. This reveals that the lower frequencies are basically coherent across the array and are preserved even after time shifting.

The results of prefiltering and beamforming TFO digital recordings of four teleseismic events indicate that:

1. The P phase from strongly recorded events is attenuated only slightly by beamforming. However, it appears that the weaker the event, the greater the loss.
2. The rms of the noise is reduced by 11-14 db, depending upon the filter, after summing.
3. The zero-to-peak maximum noise excursion in a 100-second window is about three times that of the rms obtained from the same sample.

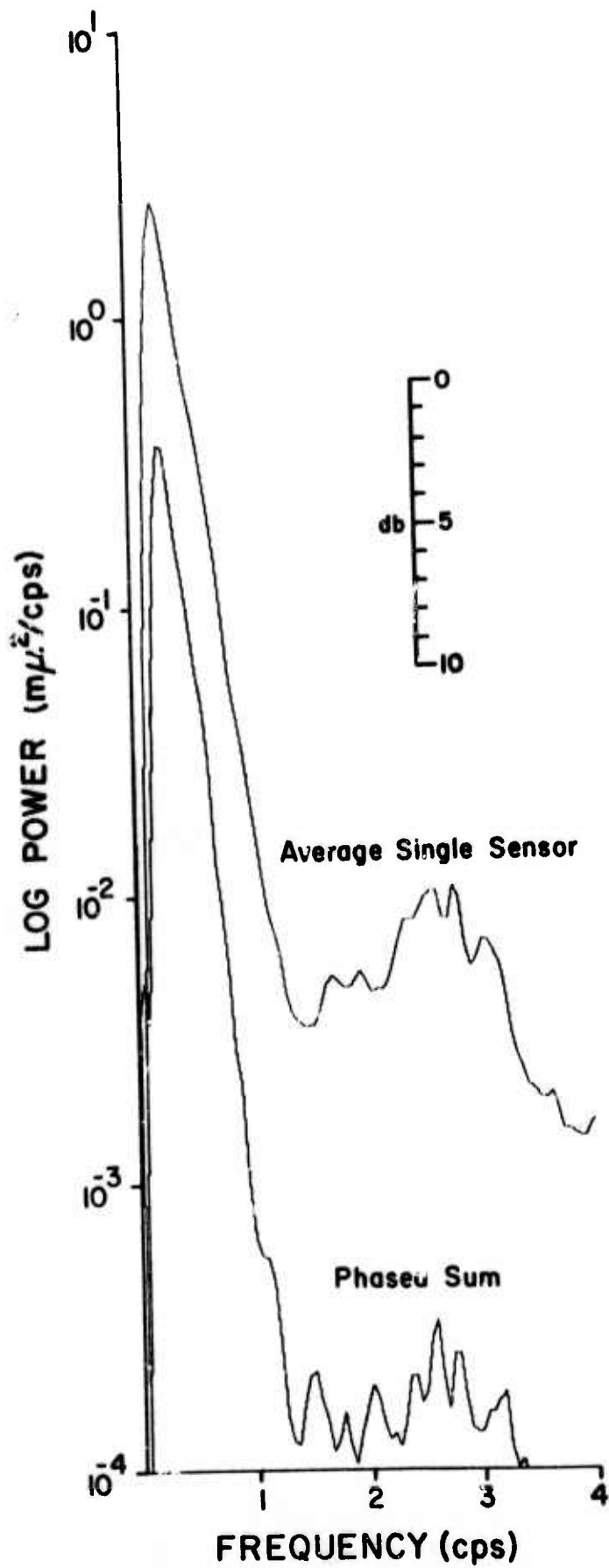


Figure 6. Power Spectra of unfiltered noise Hokkaido, 25 February 1968.

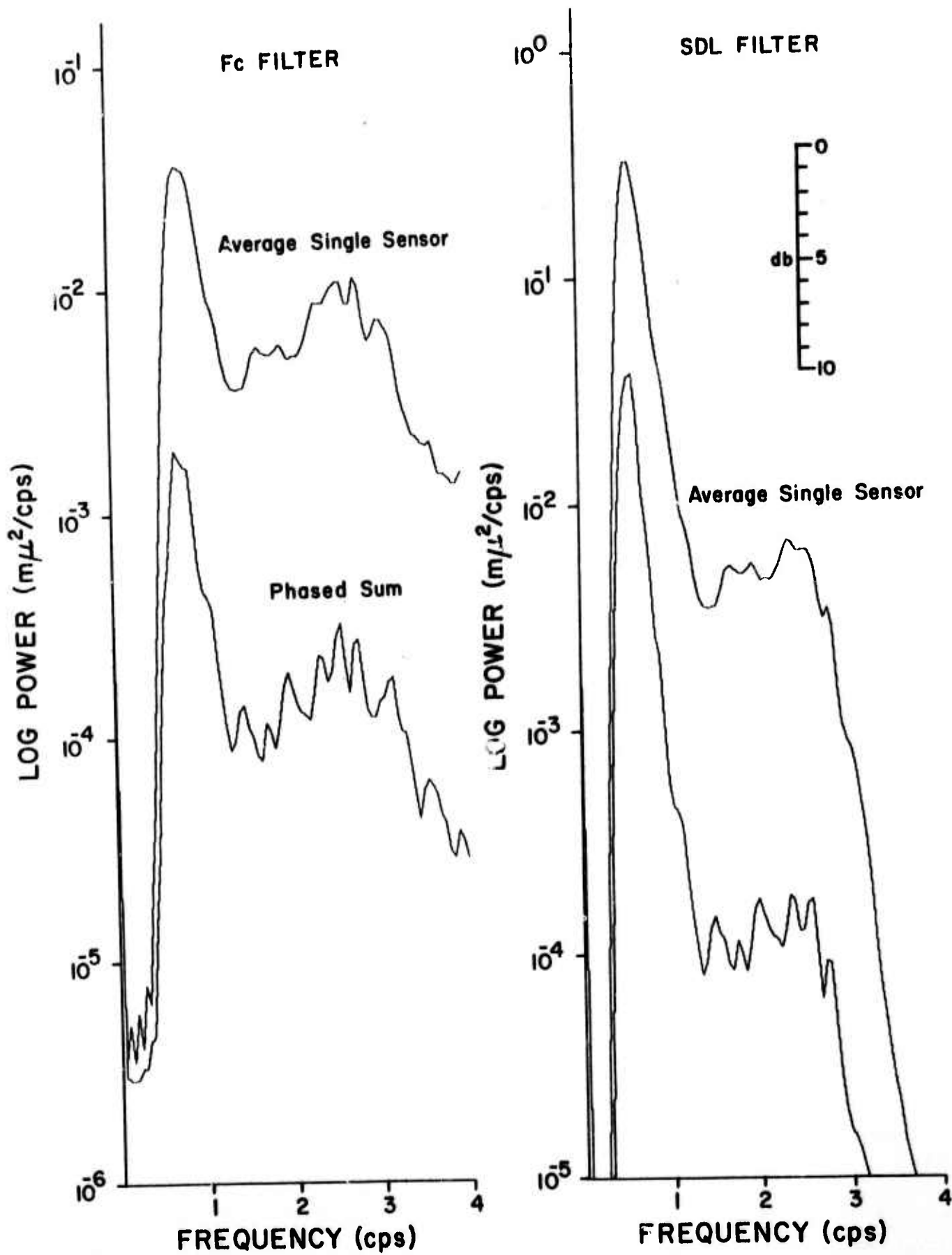


Figure 7. Noise power spectra, Hokkaido, 25 February 1968.

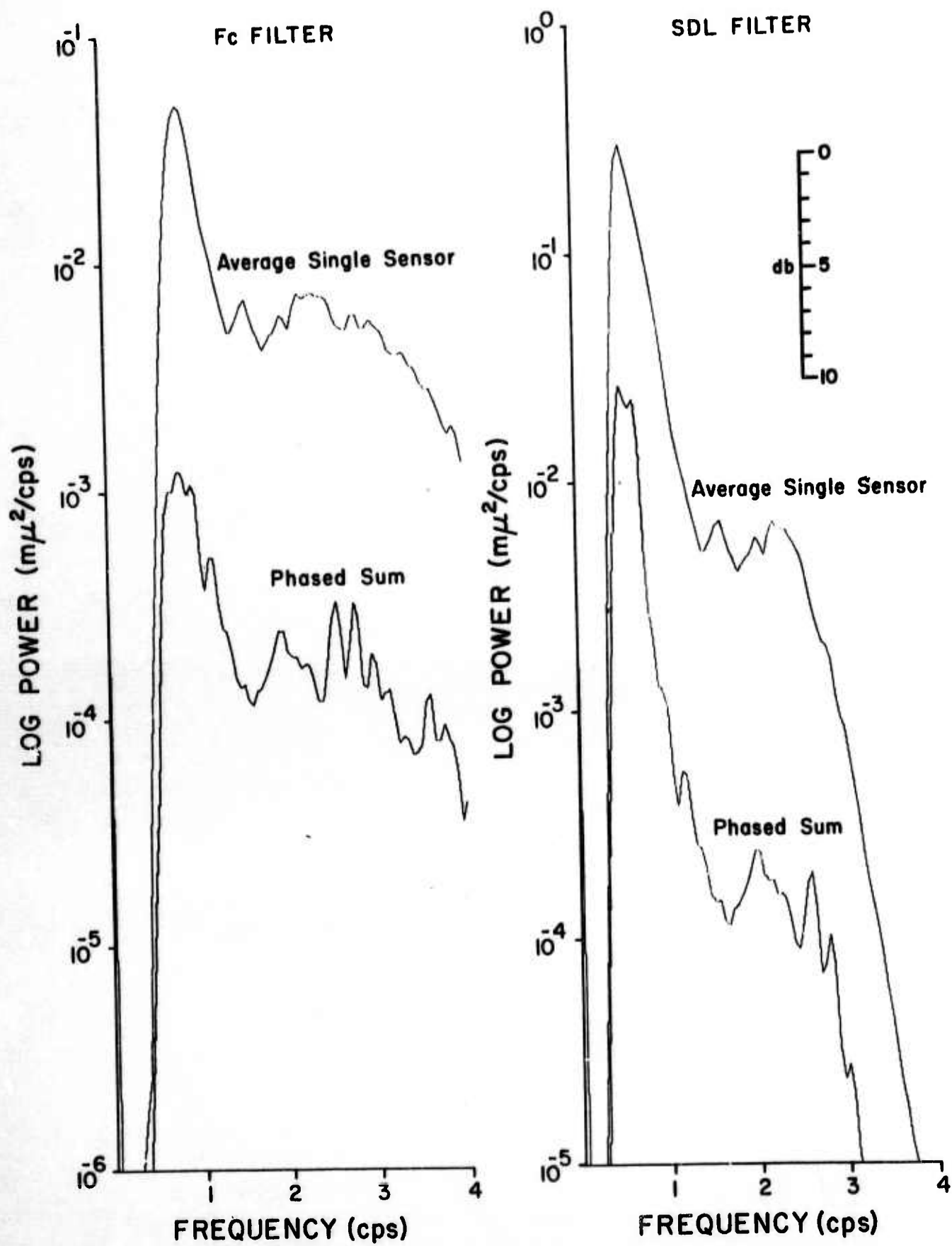


Figure 8. Noise power spectra, South Pacific, 24 February 1968.

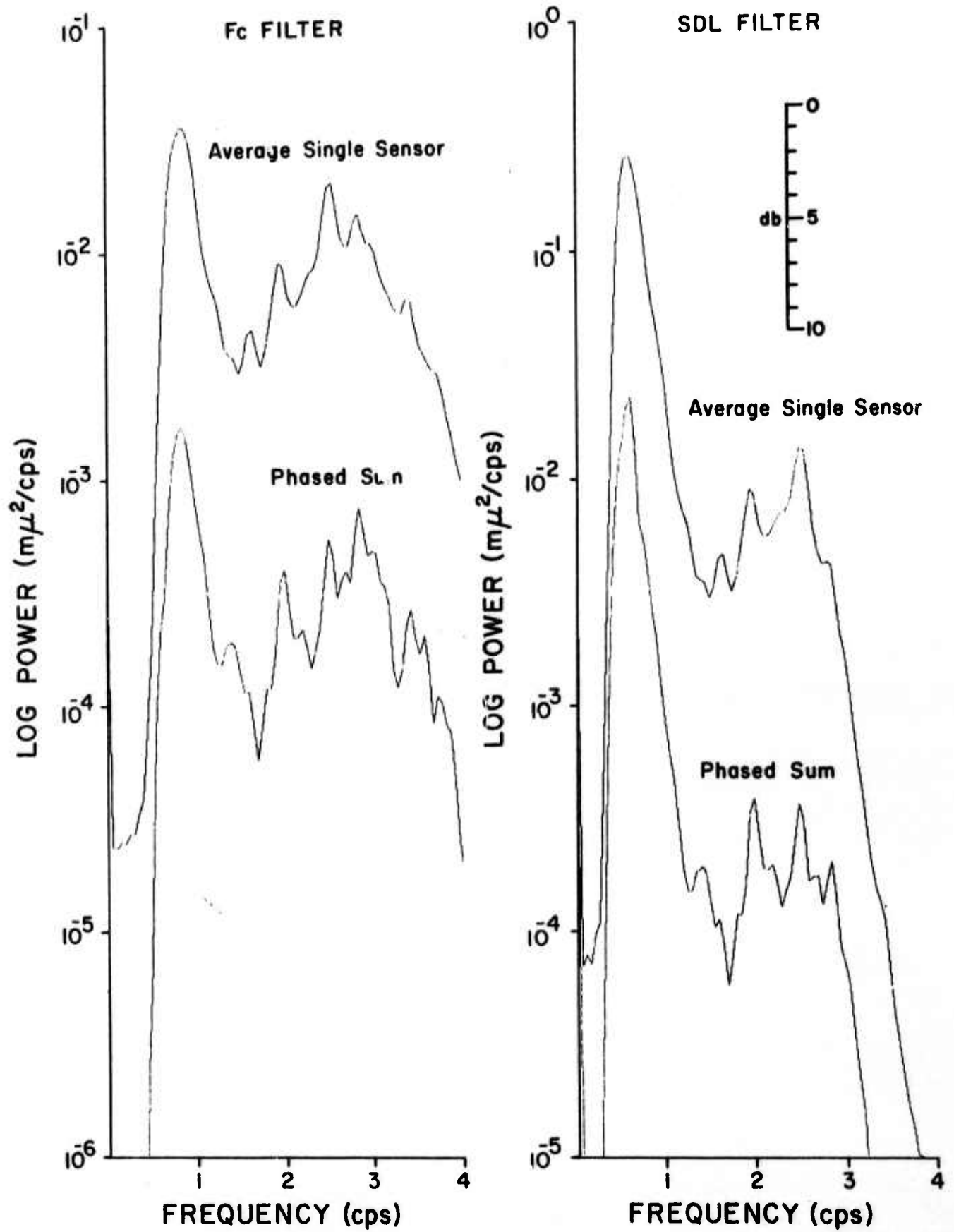


Figure 9. Noise power spectra, Peru,
24 February 1968.

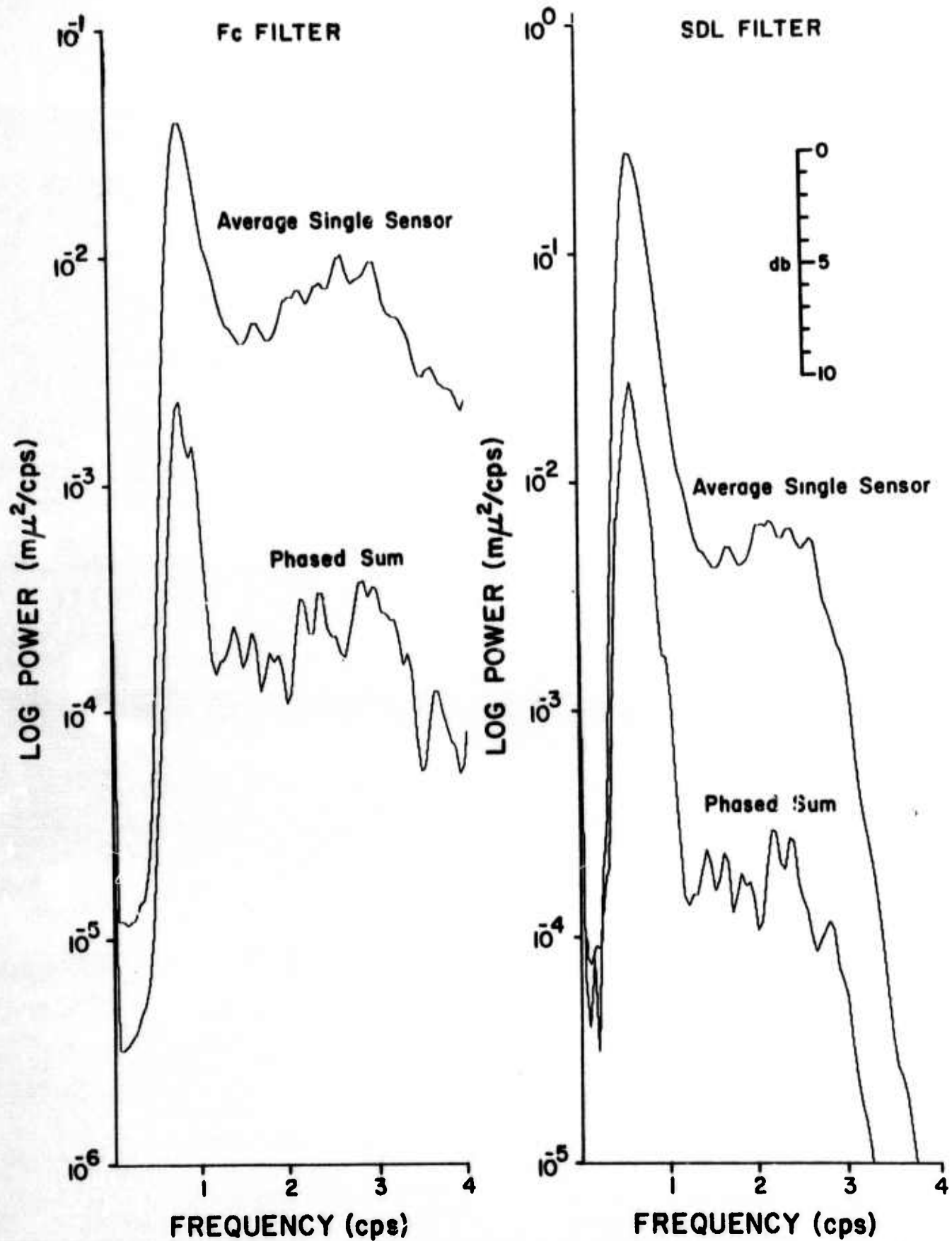


Figure 10. Noise power spectra, Tunisia, 25 February 1968.

4. There is also an 11-14 db improvement in S/N ratio by beamforming.

5. Beamforming produces about 15 db noise reduction at 1 cps as shown by the power spectra.

6. Neither filter used is completely satisfactory. The SDL seems to preserve signal amplitude at the expense of character, but does not reduce the noise to a minimum. The Fc filter reduces the noise almost to the system background, but attenuates the signal amplitude while preserving the first motion and shape.

As a result of this study, three areas of interest are indicated which should be investigated; they are:

1. The use of average observed travel-time anomalies and cross-correlations to reduce beamforming signal loss.

2. The design and evaluation of a set of bandpass filters to determine the most efficient with respect to signal preservation and noise reduction.

3. The comparison of TFO-37 with LASA, NORSAR and the other arrays in terms of their respective detection and identification capabilities.

C. P Wave Parameters Measured at the Montana LASA

The observed times of first arrival P-waves recorded by a horizontal array of seismometers such as the one at LASA provide measurements that can be used to compute (1) the reciprocal horizontal phase velocity (p), and (2) the deviation of direction of arrival. The raypath parameter p is the magnitude of the slope of the travel-time curve, and the azimuth deviation is the angle between the back azimuth to the epicenter and the apparent arrival direction. Both of these wavenumber parameters yield information about the crust and upper mantle structure beneath the array and the variation of velocity in the mantle.

The first step in computing these quantities is to fit a plane wave front to the first arrival P-waves. This was done by the least-squares method described in the original report. Making the assumption that the wave front is planar imposes the following practical limitations on events studied: (1) the events which can be considered must occur at distances greater than 2900 km (26°) from the array; (2) the maximum dimension of the array must be less than 100 km as measured from the reference station.

The errors due to scatter in observed times can be reduced to a minimum by using an array with the largest possible diameter. The F-ring of subarrays at LASA has a diameter of 200 km, which is ideally suited for this purpose.

The raypath parameter, p , and the azimuth deviation have been computed for over 600 earthquakes recorded at LASA during its first two years of operation. The epicenters of 247 events are located along a profile extending to the northwest in the range of azimuth 300° - 320° . These are so distributed as to provide essentially continuous coverage of the distance range 26° - 97° .

To reduce scatter in p and the azimuth deviation we consider only 171 events which satisfy the following criteria: (1) the event must have been clearly recorded at the reference station, A0, and at all four of the stations in the F-ring of subarrays (because the determination of the least-squares source of an event located within this range of azimuth critically depends upon the delay times at subarrays F2 and F4); (2) the event must have been recorded at least at eight of the other 16 subarrays.

Figure 11 shows the variation with distance of measured azimuth deviations along the northwest profile. The two important features of the observed variation are: (1) the average value of the azimuth deviations for all events along this profile is -0.5° , and (2) the variation in the azimuth deviations reflects the change in epicentral azimuth of these events. This becomes apparent when we examine the azimuth deviations as a function of azimuth along the profile.

For the northwest profile the epicenters in the distance range 32° and 47° are within the azimuth range 300° - 305° . All but four of the corresponding azimuth deviations have values between -0.5° and -2.0° . In the distance range 52° - 75° all but one of the epicenters are between the azimuths 310° and 317° , and all but three of the azimuth deviations corresponding to these events are between -0.5° and $+1.1^{\circ}$. In addition, the value of the azimuth deviations changes most in the distance intervals 26° - 32° , 47° - 52° , and 75° - 97° where the corresponding epicentral azimuths are undergoing the most change.

Figure 12 shows the variation of p with distance for events in the northwest profile. The observations provide almost complete coverage between 26° and 97° . With the exception of the abrupt discontinuity in the curve at 87° , all but five of the observed values of p are within ± 0.05 seconds per degree of the smooth curve fitted to the average value. The discontinuity which occurs at 87° is discussed below.

This curve can be compared with the similar curve which Chinnery and Toksöz (1967) constructed from a smaller number of events along the same profile. The curve that we present includes 171 events for which the delay times at all

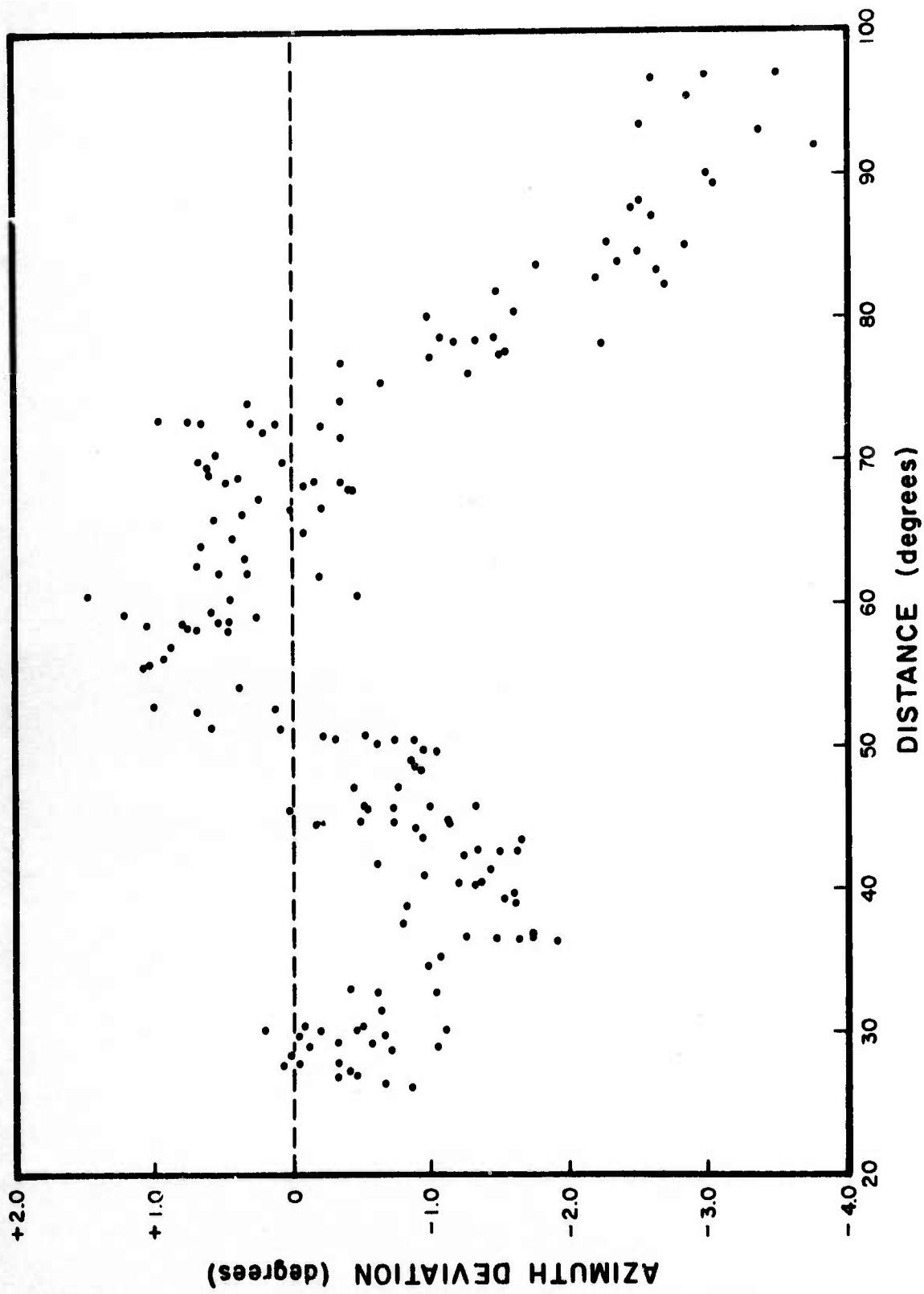


Figure 11. Observed azimuth deviations for events with epicenters located along the northwest profile, 300°-320°.

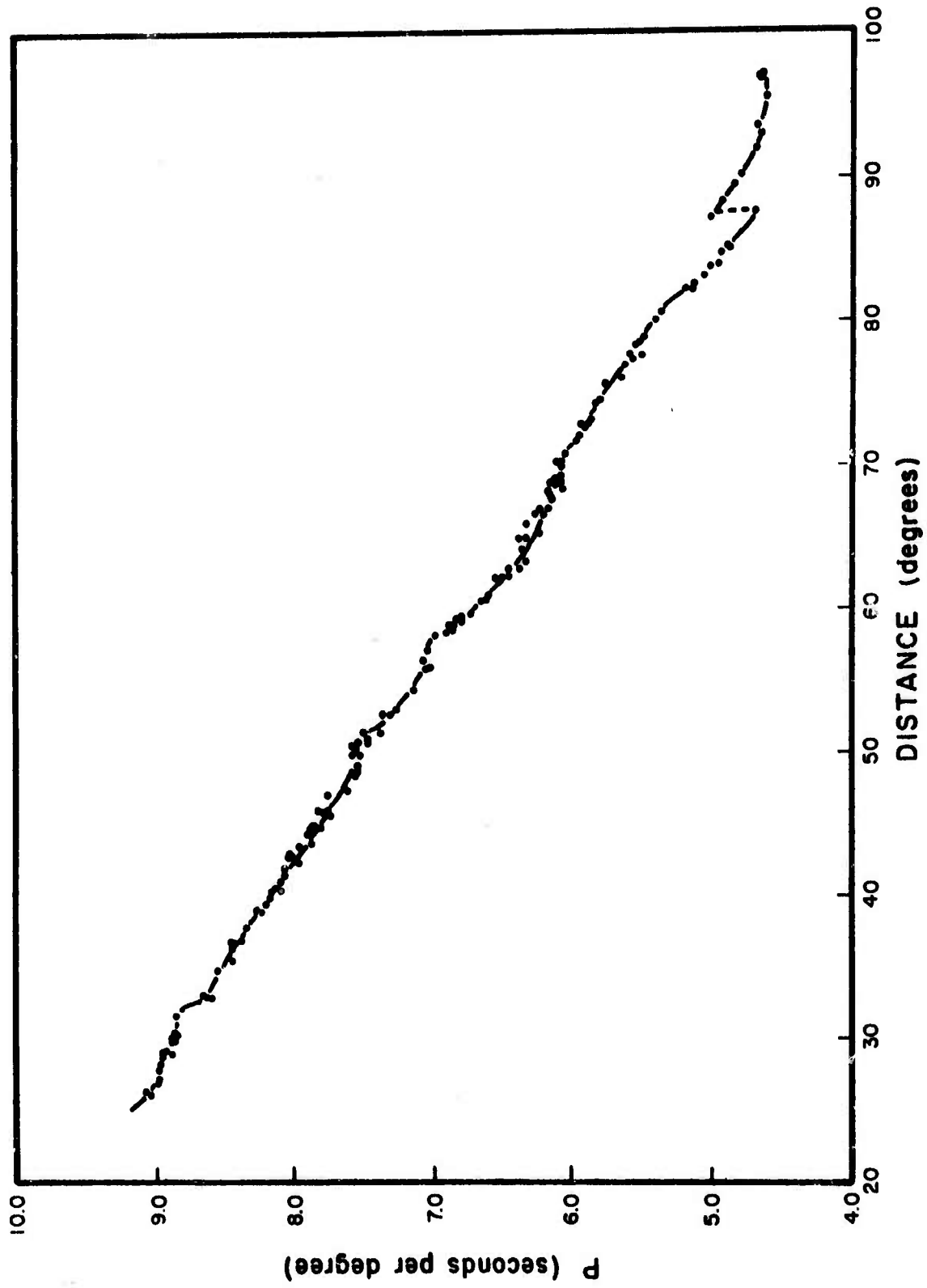


Figure 12. Observed values of p for events with epicenters located along the northwest profile, 300°-320°.

four stations in the F-ring of subarrays are available; Chinnery and Toksöz (1967, p. 204) included only 78 events on their curve. Our data are more complete in the intervals between 32° - 40° , 51° - 55° , and 72° - 78° , which are of particular interest.

Figure 13 shows the comparison between a smooth curve fitted through our observed points and the corrected observations given by Chinnery and Toksöz (1967, Table 1, p. 215-216). For reference, Figure 13 also shows the Jeffreys-Bullen curve. Our curve includes only small adjustments required for smoothing. The Chinnery-Toksöz curve includes a constant correction of +0.05 seconds per degree to make the observations consistent with the absolute travel-times (see Chinnery and Toksöz, 1967, p. 214). The Jeffreys-Bullen curve was computed by fitting a 7-point polynomial to the J-B travel-times (see Chinnery and Toksöz, 1967, p. 204).

Comparison of the two observed curves shows three intervals in which Chinnery and Toksöz (1967) extrapolated their values (32° - 40° , 51° - 55° , and 72° - 78°). The additional points on our curve demonstrate that the curve actually lies below the position that they suggest. In the intervals 32° - 40° and 72° - 78° , where their curve is projected above the corresponding portions of the J-B curve, the new data establish that the observed curve follows these portions of the J-B curve much more closely. For the interval between 52° - 55° , where Chinnery and Toksöz place their curve only slightly below the J-B curve, our additional points suggest that this portion of the observed curve falls well below the Jeffreys-Bullen curve. The remaining portions of our curve, out to a distance of 87° , are in good agreement with Chinnery and Toksöz, except for the correction of +0.05 seconds per degree. This correction has not been added to our curve.

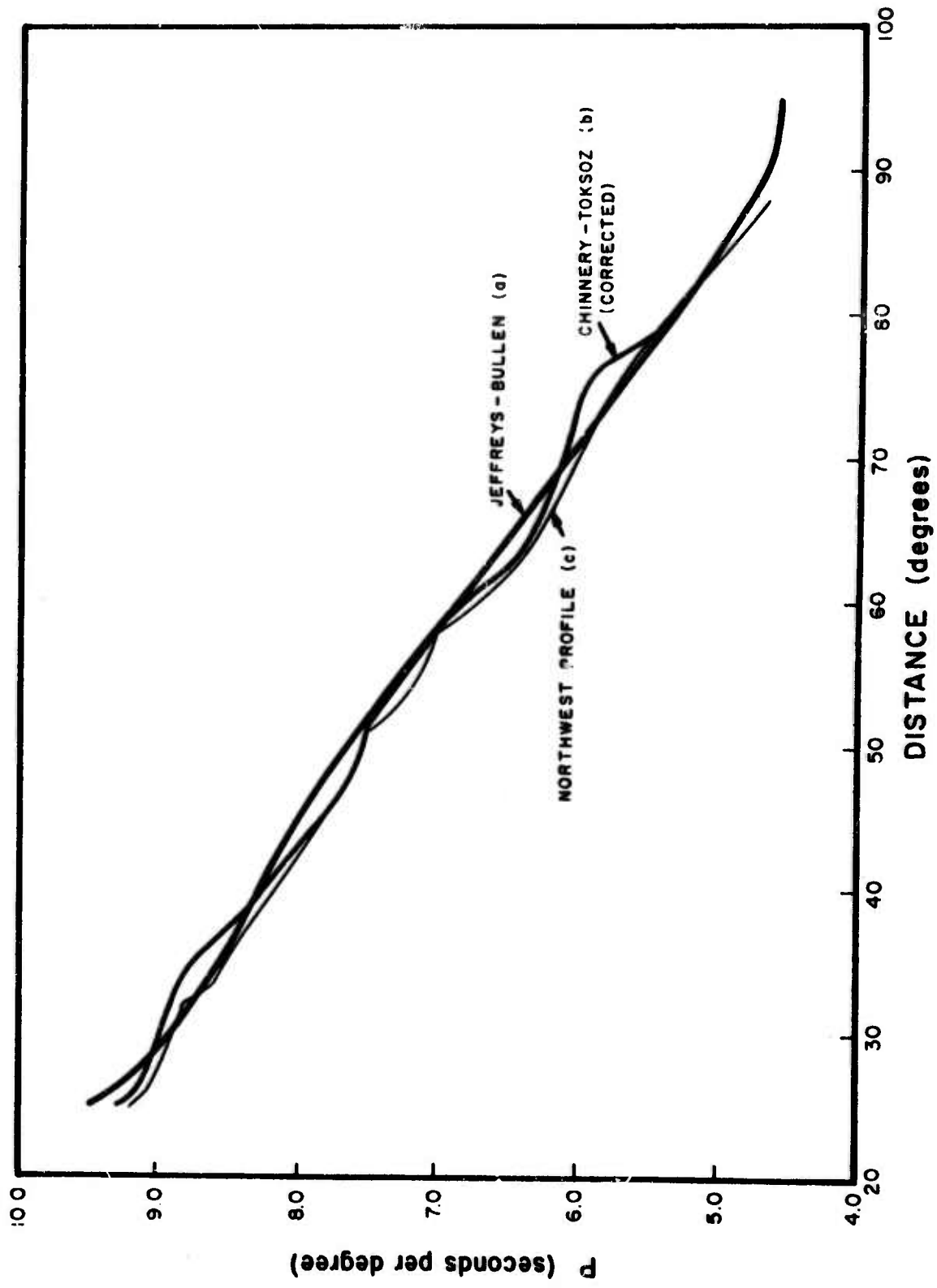


Figure 13. p versus distance curves

The segments along our curve which differ from the Chinnery-Toksöz curve are of particular interest. Chinnery and Toksöz (1967, p. 233) conclude from their results that the points where the slope increases abruptly (35° , 52° and 70° on their curve) reflect points of inflection in the velocity-depth function. They further conclude that these points of inflection occur at depths of approximately 800, 1300, and 2000 kilometers, respectively. The new detail provided by our values of p shows abrupt slope increases at 32° , 51° , 58° , and 71° . Our data thus indicate that: (1) on the northwest profile an additional point of inflection occurs in the velocity-depth function at a depth of approximately 1500 kilometers, and (2) the upper point of inflection occurs at a depth of approximately 750 kilometers.

Because our values of p were determined using only first arrivals they do not show any travel-time triplications directly, but they do show two features expected at triplication distances. These are: (1) relative absence of points where the slope increases rapidly, which may result from the reduced amplitude of the P wave arrival where triplication occurs; (2) relative abundance of points in the interval immediately preceding the change in slope, as a result of focusing by the bottom of the velocity transition layer. Our curve shows a concentration of points in the intervals $29^\circ-31^\circ$, $49^\circ-51^\circ$, $56^\circ-57^\circ$, and $68^\circ-71^\circ$ and a corresponding lack of points in the intervals $31^\circ-33^\circ$, $51^\circ-53^\circ$, $57^\circ-58^\circ$, and $71^\circ-72^\circ$.

The abrupt discontinuity in the curve of p vs. distance for the northwest profile at 87° is probably due to a large change in epicentral azimuth of the corresponding events. All

of the p values in the interval 83° - 88° fall on the lower portion of the curve and the corresponding epicenters are in the range of azimuth 300° - 308° . The epicentral azimuths of all the events in the distance interval 87° - 97° , where the p values fall on the upper portion of the curve, are between 309° and 314° . Thus, the systematic change in the p-distance curve reflects a systematic change in the corresponding epicentral azimuths along the northwest profile.

The southeast profile includes 122 events in the range of azimuth 140° - 160° . Forty other events whose epicenters lie on the profile were omitted because one or more stations in the F-ring did not record the signal. The 122 events finally included in the southeast profile satisfy all of the criteria for quality stated in the previous section.

Figure 14 shows the variation with distance of measured azimuth deviations along the southeast profile. Two important observations about azimuth deviations along this profile are: (1) the average value of $+1.0^{\circ}$, and (2) a strong relationship with epicentral azimuths.

In the distance interval 38° - 72° all of the epicenters are in the range of azimuth 142° - 150° and all but three of the related values for azimuth deviations are between $+0.9^{\circ}$ and $+2.5^{\circ}$. In the distance intervals 31° - 38° and 72° - 97° , where the epicentral azimuths change by more than 10° , the corresponding azimuth deviations also undergo the greatest rate of change.

Comparison of Figure 14 with Figure 11 shows that the azimuth deviation along the southeast profile is greater than along the northwest profile by at least 1.5° . This demonstrates a strong function of azimuth along both profiles.

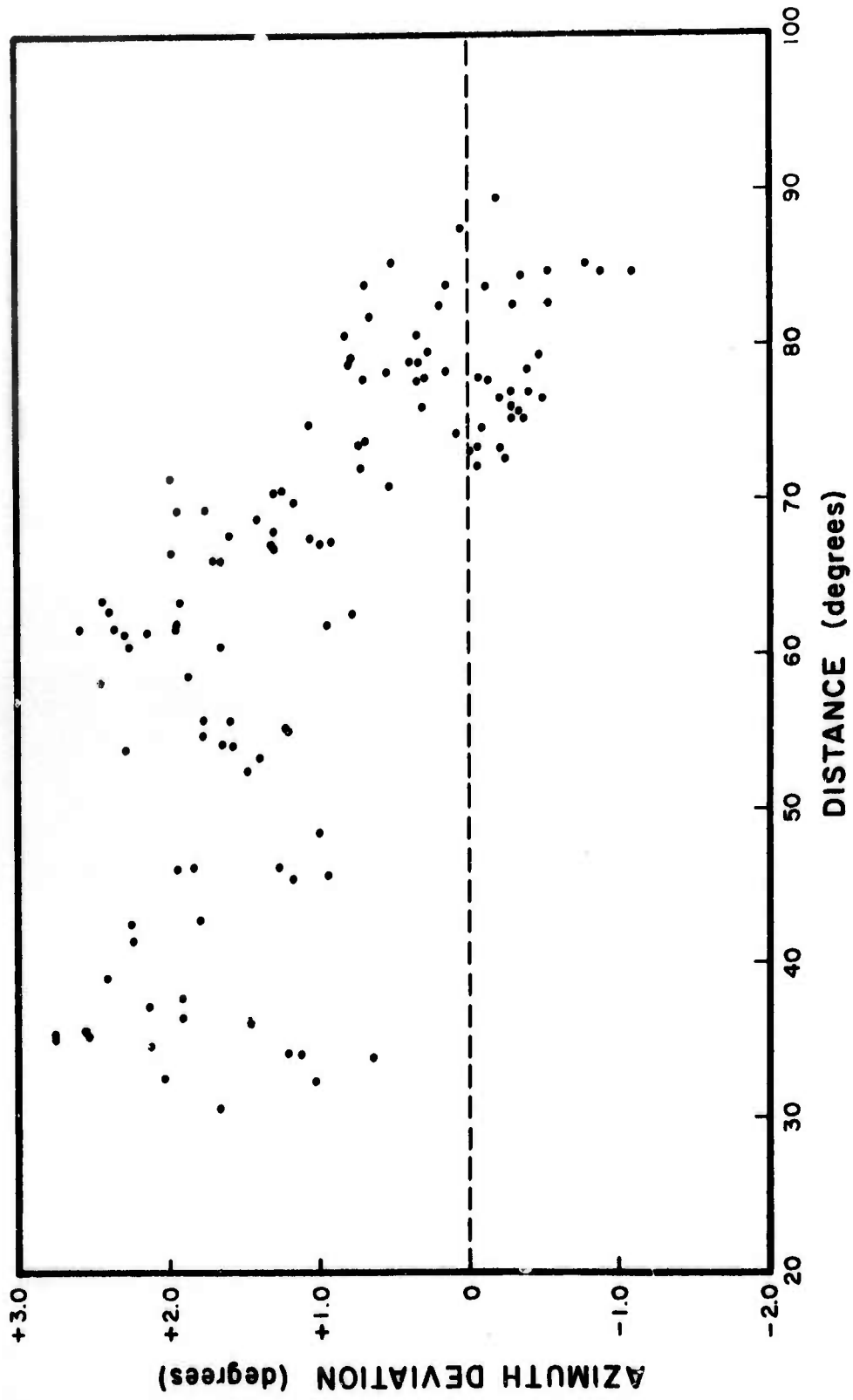


Figure 14. Observed azimuth deviations for events with epicenters located along the southeast profile, 140°-160°.

Figure 15 shows the variation of p with distance for events along the southeast profile. The observed points provide good coverage of the distance range between 31° and 86° with the exception of the intervals between $39^\circ-42^\circ$, $43^\circ-45^\circ$, $47^\circ-52^\circ$, $56^\circ-60^\circ$, and $63^\circ-66^\circ$. Five observed points in the interval $86^\circ-97^\circ$ establish the approximate position of this portion of the curve. All but four of the observed points along the southeast profile are within ± 0.08 seconds per degree of the smooth curve fitted to the average value.

The lack of observed data in the above intervals creates some doubt as to the actual position of the curve in these intervals. However, available data do show the following features along the southeast profile: (1) An abrupt increase in slope or an actual triPLICATION is clearly indicated in the distance interval $34^\circ-35^\circ$; (2) Similar abrupt increases in slope or triPLICATIONS are suggested in the distance intervals $49^\circ-54^\circ$ and $63^\circ-66^\circ$; (3) The distance interval $39^\circ-42^\circ$ may include such an abrupt increase in slope; (4) There are no clear indications of abrupt increases in slope at distances 32° , 58° , or 71° , where increases in slope were observed on the northwest profile.

Figure 16 shows a smooth curve fitted to p observed along the southeast profile, together with the observed curve for the northwest profile. The extrapolated distance intervals are shown by broken lines. Comparison of the two curves shows that the southeast profile curve is displaced from the northwest profile curve by an amount 0.48 seconds per degree, on the average. The position of the curve from the southeast profile after a constant correction of -0.48 seconds per degree has been applied is also shown in Figure 16.

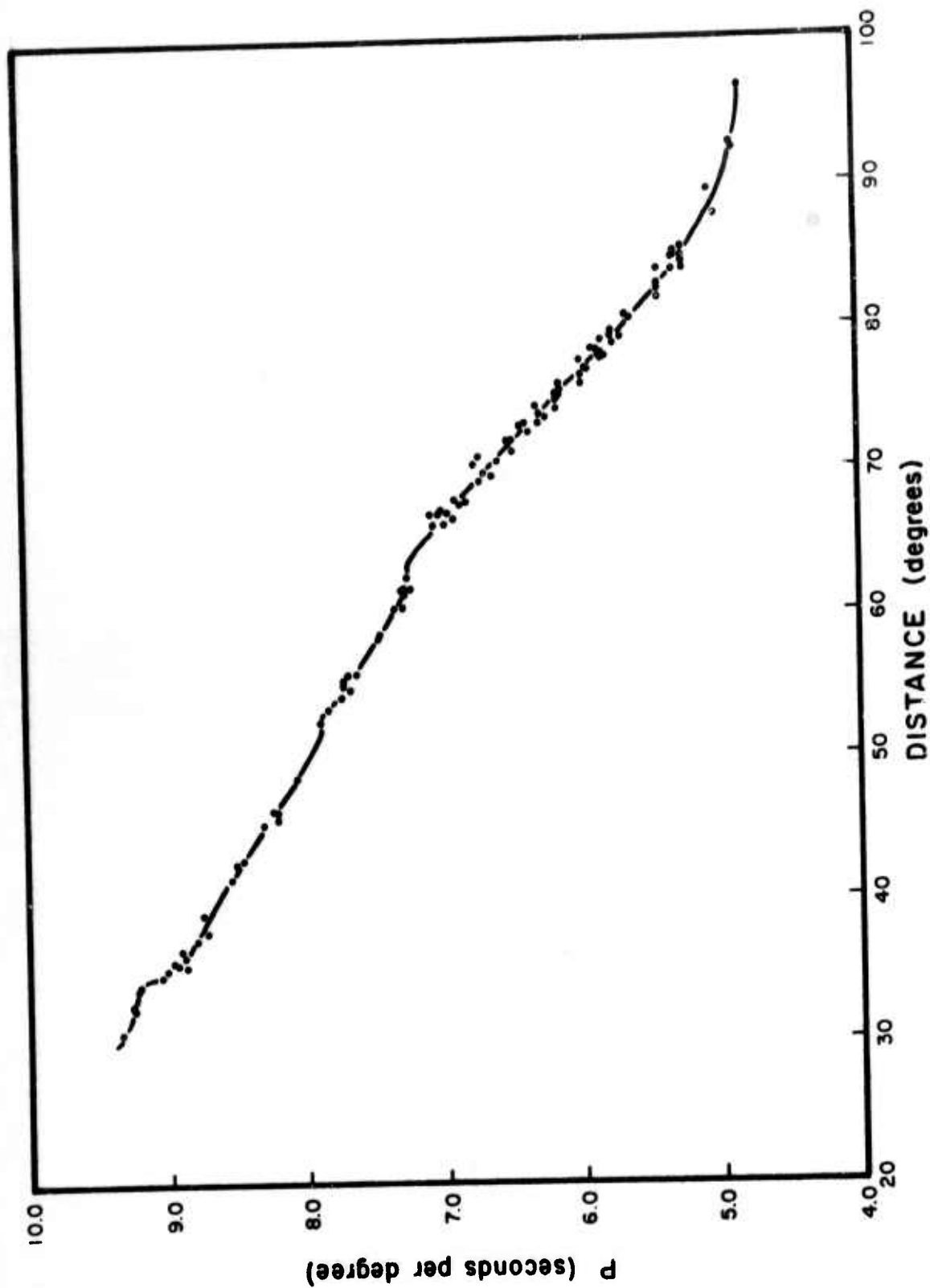


Figure 15. Observed values of p for events with epicenters located along the southeast profile, 140°-160°.

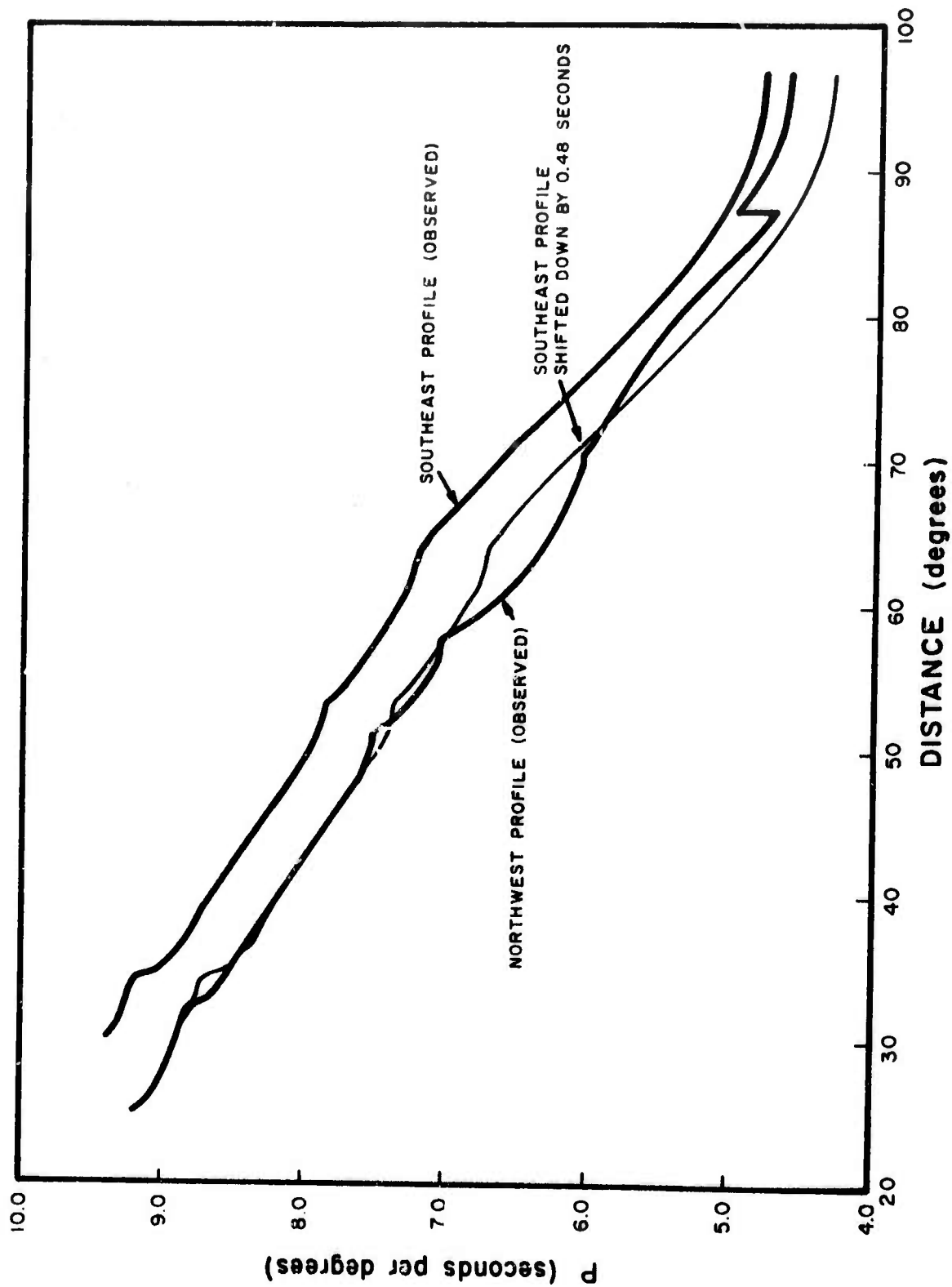


Figure 16. p versus distance curves

Comparison of the northwest profile with the southeast shows: (1) the abrupt increases in slope which are clearly indicated at 32° and 71° on the northwest profile are not at all suggested by the data available from the southeast profile; (2) there are abrupt slope increases along the southeast profile in the intervals 34° - 35° and 63° - 66° which are clearly not indicated for the same intervals on the northwest profile; (3) it is possible that the abrupt increases in slope which occur at 51° and 58° on the northwest profile also occur at the same distances along the southeast profile, although the sparse data from the southeast profile suggest that such a change does occur between 53° and 54° but does not occur between 56° and 62° .

As for the northwest profile, each place where the p versus distance curve has an abrupt increase in slope reflects a corresponding increase in the velocity-depth function. Present data from the southeast profile do not provide enough detail in the critical distance intervals to determine the actual depths at which these velocity transition zones occur. However, these data strongly suggest that three such velocity transitions occur beneath the southeast profile, at corresponding depths of approximately 800, 1350 and 1800 kilometers (these depth estimates are crude interpolations made using the figures of Chinnery and Toksöz, 1967). Similar transition zones have been previously observed in the upper mantle by many other workers (for example, Archambeau *et al.*, 1967; Johnson, 1967; Anderson, 1967).

The average value of the observed azimuth deviations along the southeast profile is 1.5° greater than that for the northwest profile, and the observed p values for the southeast profile are greater than those for the northwest profile by nearly 0.5 seconds per degree. In addition, the observed discontinuity at 87° in the p curve for the northwest profile is apparently related to a systematic change in the epicentral azimuths. These observations show that both wave-number parameters change considerably with changes in epicentral azimuth.

Azimuthal changes of this kind can result from either dipping layers or horizontal velocity gradients within the crust and upper mantle beneath the array. From a study of the relative station corrections at LASA, Fairborn (1966) has concluded that dipping layers cannot account for the magnitude of the required corrections but that horizontal velocity gradients may account for the required magnitude if they extend into the upper mantle. Thus we conclude that the azimuthal variation in p and azimuth deviation is probably caused by horizontal velocity gradients beneath LASA which extend into the upper mantle.

The observed variation with distance of p along both the northwest and southeast profiles shows abrupt increases in the slope of the curve at several places. However, the distances at which these changes occur are not the same along the two profiles. The additional detail provided by the new data from this study for the northwest profile suggests that abrupt increases in the slope of the p distance curves reflect several previously observed velocity increases within the mantle.

For the northwest profile, our data indicate that four such velocity transition zones occur, at depths of approximately 750, 1300, 1500, and 2000 kilometers. For the southeast profile the data are not as detailed, but they suggest that at least three such velocity zones occur at depths of approximately 800, 1350, and 1800 kilometers. Thus, the new data presented here demonstrate that the velocity-depth function for the region extending northwest from LASA is distinctly different from that for the region to the southeast for depths between 700 and 2000 kilometers.

Departures of times from the least-squares plane wave front are the stations deviations. The results suggest additional work to determine if station deviations can be obtained as a function of azimuth and distance. The variation of p and azimuth deviations shown by this study suggest that the station deviations depend mainly on azimuth. However, it is possible that they also depend on distance to some extent.

References

Anderson, D.L., 1967, Phase changes in the upper mantle: Science, Vol. 157, p. 1165-1173.

Archanbeau, C.B., Flinn, E.A., Lambert, D.C., 1967, Fine Structure of the Upper Mantle: Paper presented at the April, 1967, meeting of the American Geophysical Union.

Chinnery, M.A., and Toksöz, M.N., 1967, P-wave velocities in the mantle below 700 km, Bull. Seism. Soc. Amer., v. 57, No. 2, p. 199-226.

Fairborn, J.W., 1966, Station corrections at LASA, Dept. of Geology and Geophy., MIT, under AF-49-(638)-1632.

Johnson, L.R., 1967, Array measurements of P velocities in the upper mantle, Div. of Geol. Sci., Calif. Int. Tech., contribution No. 1469, under AF-49-(638)-1337.

D. An Analysis of a Technique for the Generation of High Resolution Wavenumber Spectra.

The technique of computing high-resolution wavenumber spectra follows the method used by Haney, (1967). The basic method consists of designing a multichannel filter whose desired output is an impulse at time $t = t_0$ and spatial lag $x = x_0$, where t_0 is usually zero and x_0 is the spatial position of one of the seismometers. The method consists of designing a least-mean-square error "whitening" filter to "whiten" the data in f-k space. The inverse of the f-k response of the filter which given a "white" or constant f-k spectrum when applied to the space-time series data should give a good estimate of the true f-k spectrum of the original data. This method could also be considered as equivalent to extending the spatial correlation functions (Burg, 1967).

The multichannel whitening filter is sensitive to gain inequalities. One method of compensation is to normalize the spectral matrix in a manner prescribed by Haney, (1967).

We further note that the expression derived in the original report for the high-resolution wavenumber spectrum for two plane waves input is quite similar to that for the spectrum of a single plane wave, with the exception that $P(f,k)$ has cross terms, and N is replaced by $R(\omega)$ in the expansion $(c + N)^{-1}$. Some of the results for a single plane wave and two plane waves input are described in the next section.

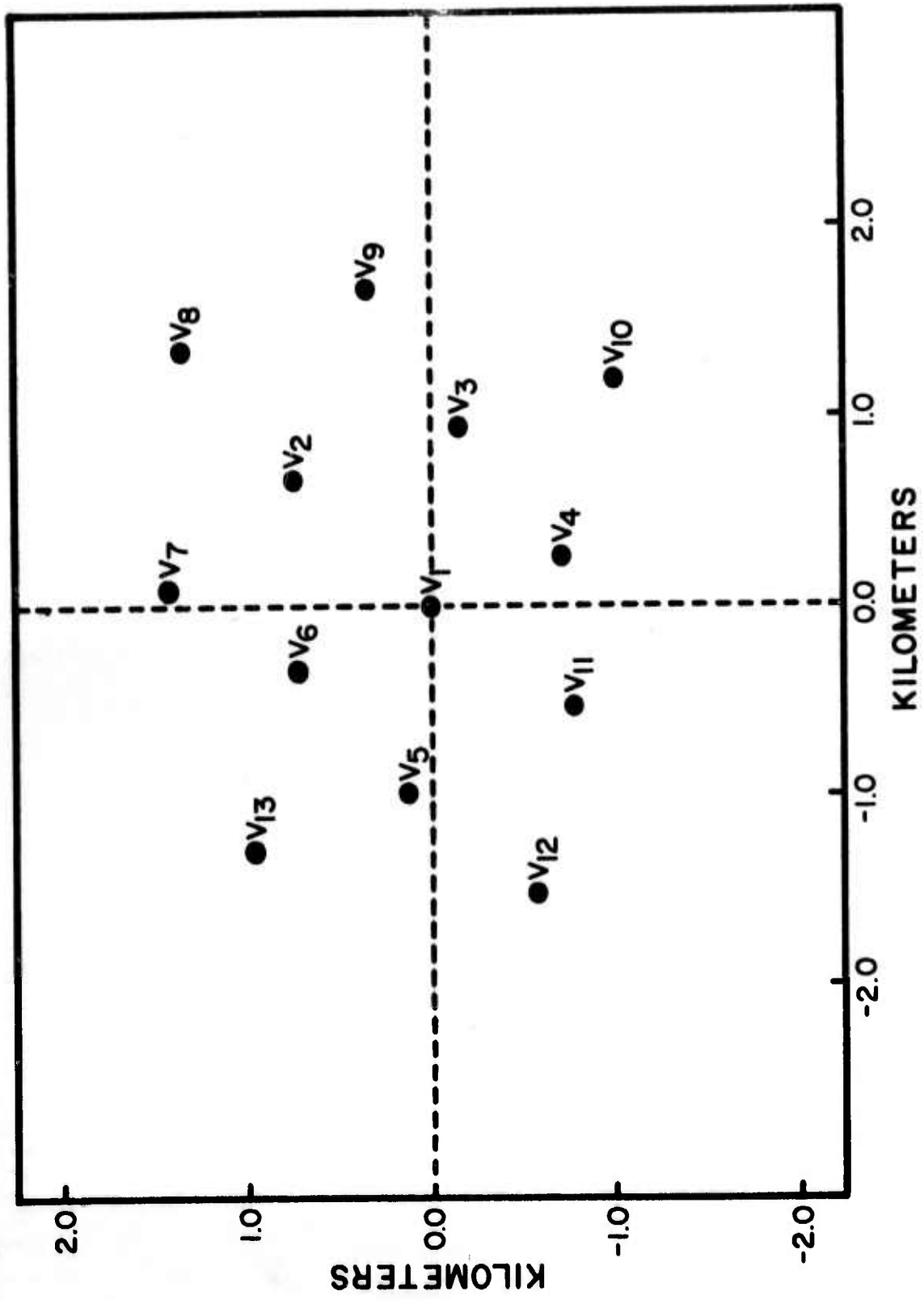


Figure 17. WMSO surface array

Figure 19 is the ordinary f-k spectrum of the 12 km/sec impulse at a frequency of .3125 cps. Figure 20 is the high-resolution wavenumber spectrum (designed on the center seismometer) for the same event at the same frequency. Comparing Figure 20 with Figure 19 we see that the high-resolution wavenumber spectrum at .325 cps indeed shows an improvement in resolution over the ordinary spectrum (Figure 19). Figure 20 shows a signal arriving from the south with a velocity of slightly greater than 10 km/sec, whereas Figure 19 (the ordinary f-k spectrum) shows a signal coming from the general direction of the south but with much uncertainty as to the exact velocity and azimuth.

Figure 21 is the high-resolution wavenumber spectrum based on the output of a WMO sensor at a frequency of .3125 cps. Comparing Figure 21 with Figure 20, we see that the resolution of the high-resolution f-k spectrum (Figure 21) is approximately equal to the resolution of the high-resolution f-k spectrum (Figure 20) obtained using the output of another seismometer; however, the spectrum in Figure 21 is "stretched" along the line perpendicular to the direction of the line connecting the two recording positions. Thus, the net result of designing a high-resolution f-k spectrum on a seismometer located at $\underline{x} = \underline{x}_0$ is to introduce a $\cos(2\pi \underline{k} \cdot \underline{x}_0)$ term, which causes a stretching of the spectrum along a direction perpendicular to the vector $\underline{x} = \underline{x}_0$. Figure 22 is the high-resolution f-k spectrum averaged over all of the seismometers in the array, for the 12 km/sec event, at a frequency of .3125 cps. Comparing Figure 22 with Figures 20 and 21, we see that in the high-resolution spectrum which has been averaged over all of the seismometers, the non-physically meaningful stretching of

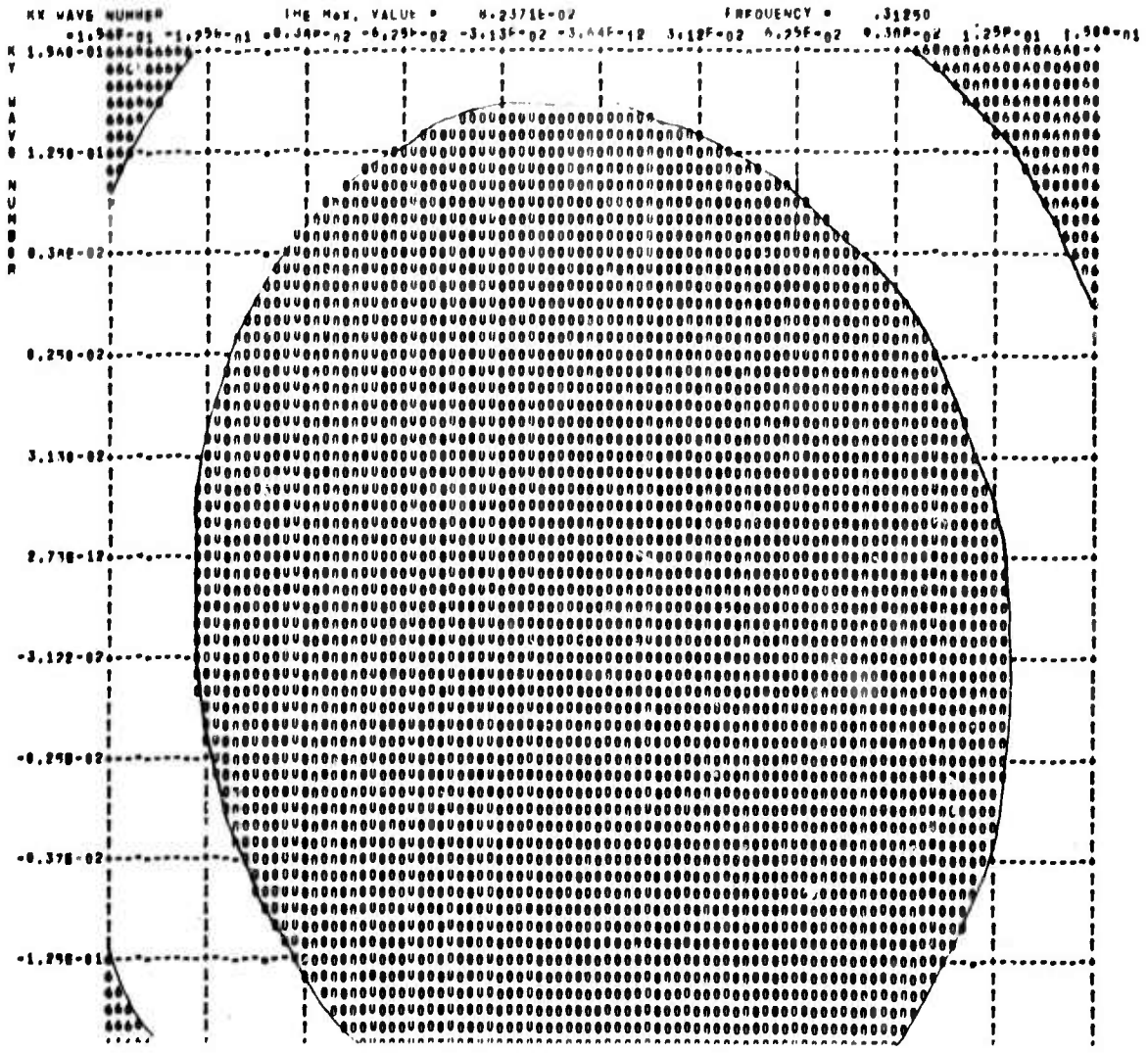


Figure 19. The ordinary f-k spectrum of a theoretical 12.0 km/sec plane wave arriving at WMO from the south; the frequency is 0.3125 cps.

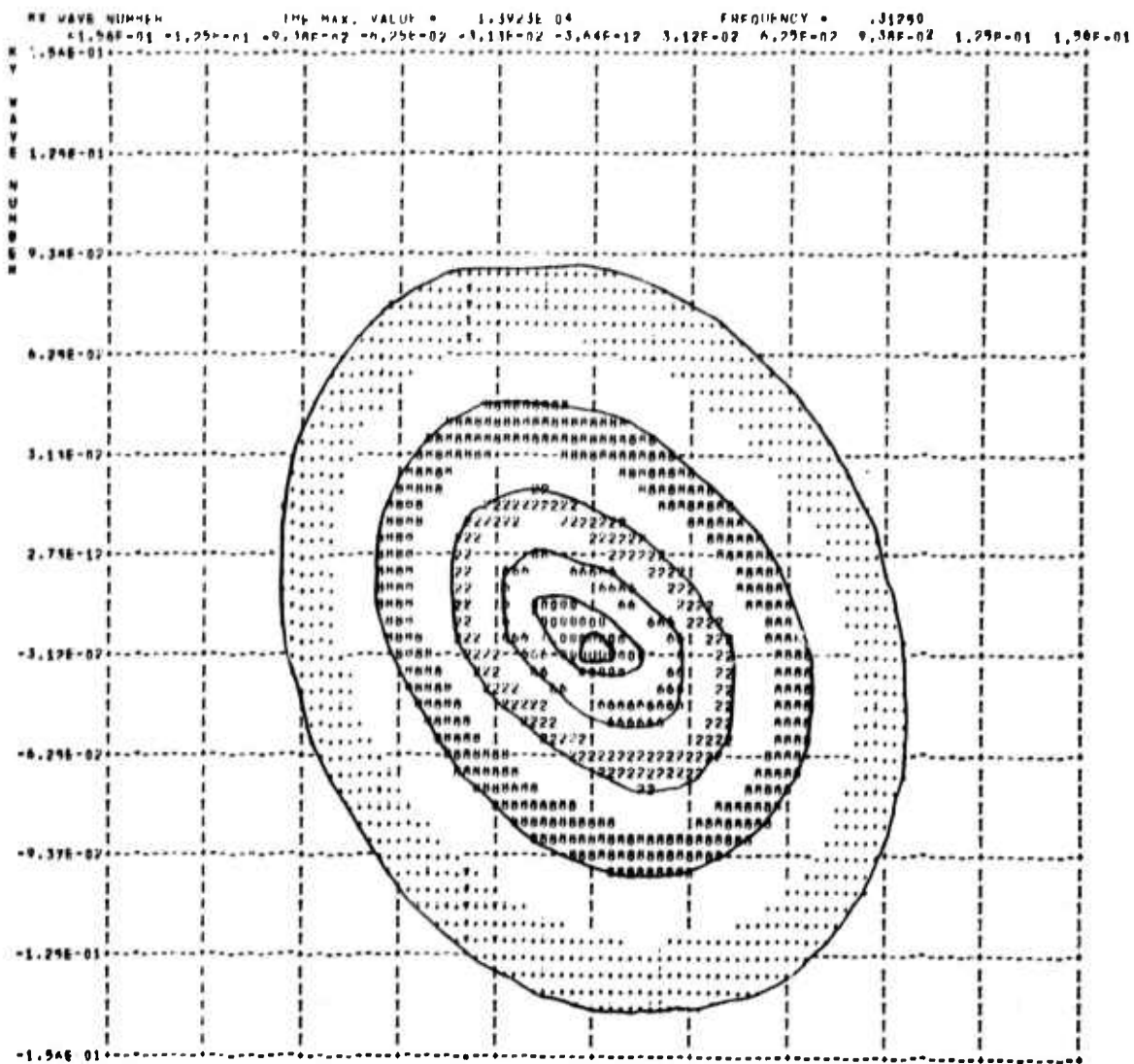


Figure 20. The high-resolution f-k spectrum of the 12.0 km/sec event at 0.3125 cps; S/N = .03.

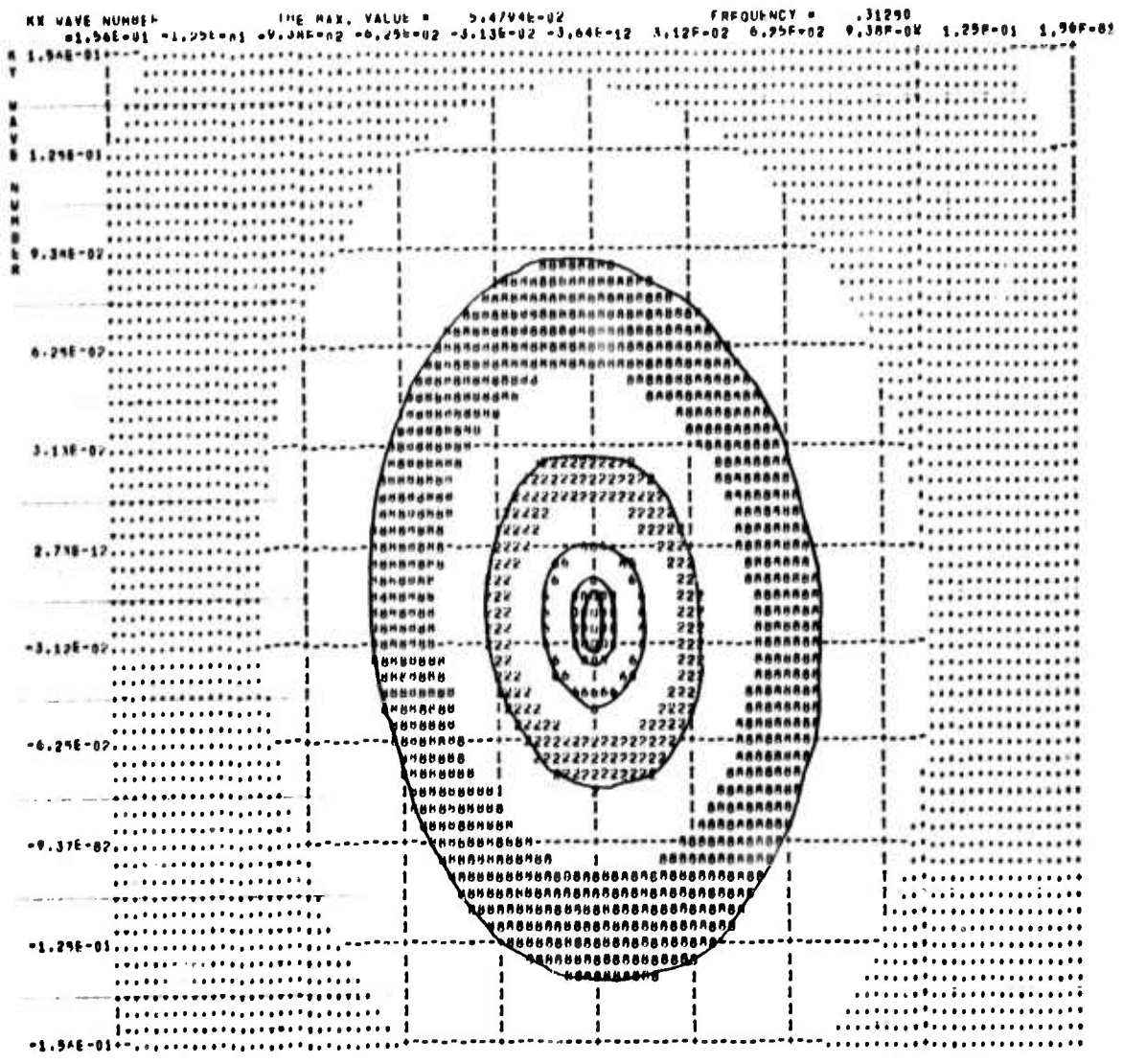


Figure 22. The high-resolution f-k spectrum for the 12 km/sec plane wave at .3125 cps averaged over all of the seismometers; S/N = .03.

the spectrum due to designing the high-resolution spectrum on an off-center seismometer has been cancelled out. The spectrum of Figure 21 is not quite as peaked as that of Figure 20, although the difference is insignificant. The spectrum of Figure 20 is also tilted to the left due to the asymmetry of the WMO array, whereas the spectrum of Figure 21 seems to be slightly "stretched" in a northwardly direction.

Figure 23 is the ordinary f-k spectrum of LONGSHOT recorded at LASA F1 at a frequency of 0.625 cps. Figure 24 is the "averaged" high-resolution f-k spectra at the same frequency. The signal-to-noise ratio (c) was 2.0. At 0.625 cps, both the averaged high-resolution (Figure 24) and the ordinary spectrum (Figure 23) indicate the event is coming from the correct direction, but the velocity is somewhat smaller than expected (11.6 $\hat{\text{km}}/\text{sec}$, vs. 14.1 km/sec, from the J-B traveltimes tables).

Figure 25 is a beam-steered (time-shift and sum) power density spectrum of LONGSHOT. Nine seismometers in-line in the approximate direction of the event were time-shifted and summed. The power spectrum of the sum was then computed and displayed in Figure 25. This demonstrates that there is enough power at 2.5 cps to give an accurate f-k spectrum at that frequency.

Figure 26 is the array response of thirteen of the seismometers of LASA XE3. Figure 27 is the ordinary f-k spectrum of a plane wave of velocity 20 km/sec and amplitude 1.0 plus a plane wave of velocity 30 km/sec and amplitude 0.2, computed at 0.625 cps. Figure 28 is the averaged high-resolution f-k spectrum (S/N = 2.0) of the same event calculated

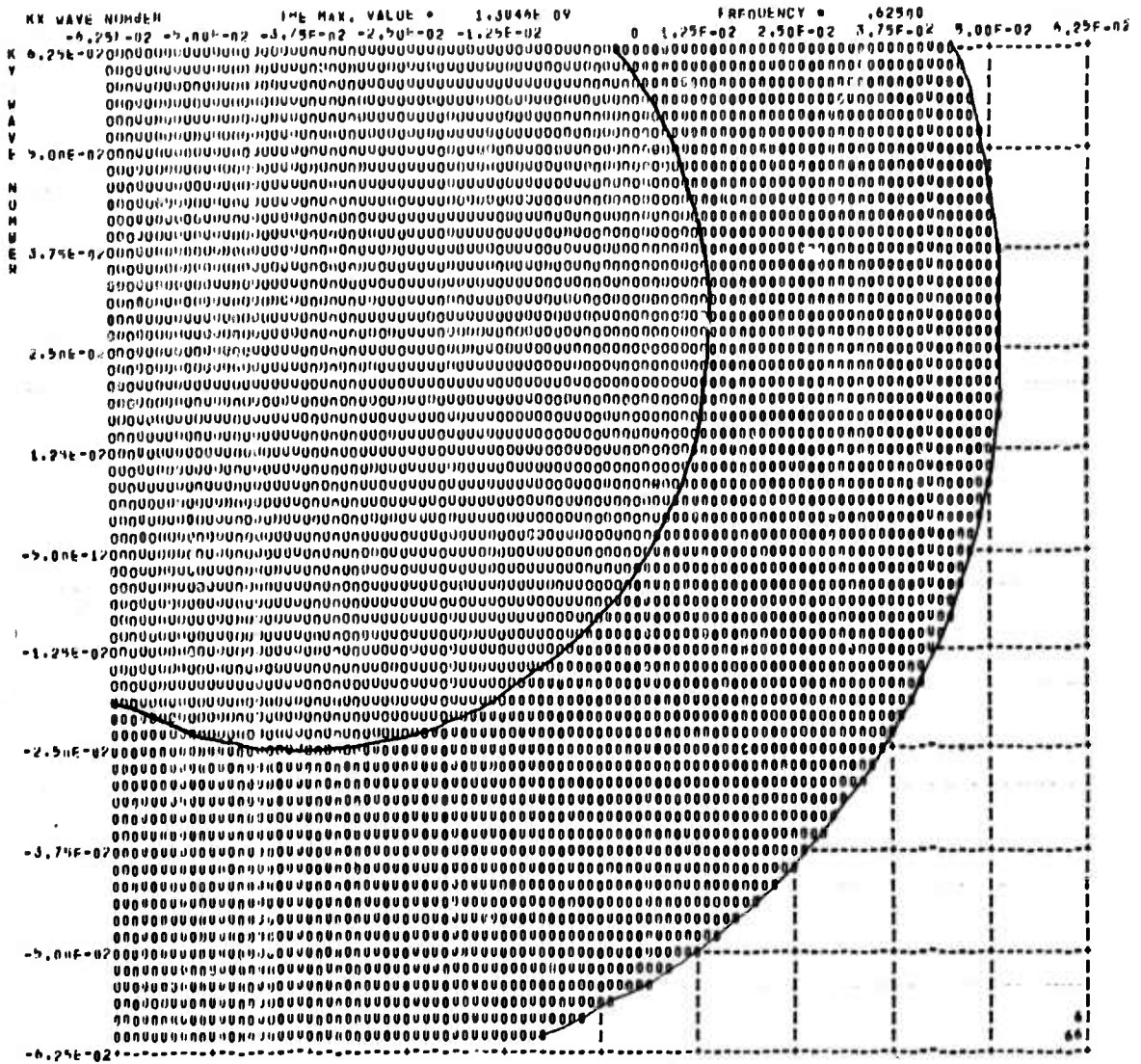


Figure 23. Ordinary f-k spectrum of LONG SHOT at LASA sub-array F1 at .625 cps.

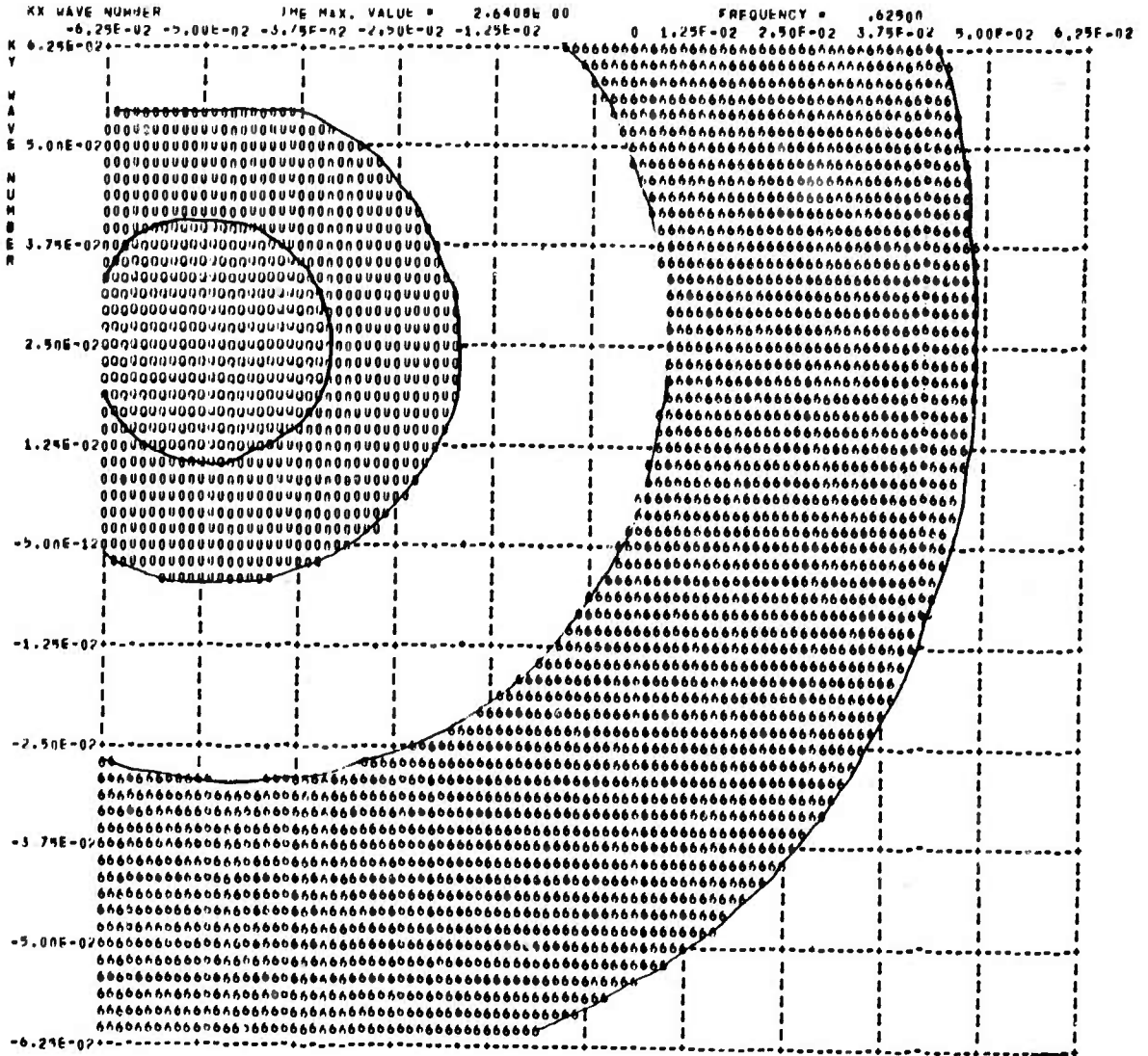


Figure 24. High-resolution f-k spectrum of LONG SHOT at LASA, F1, averaged over all seismometers in the array at .625 cps. C= 2.0

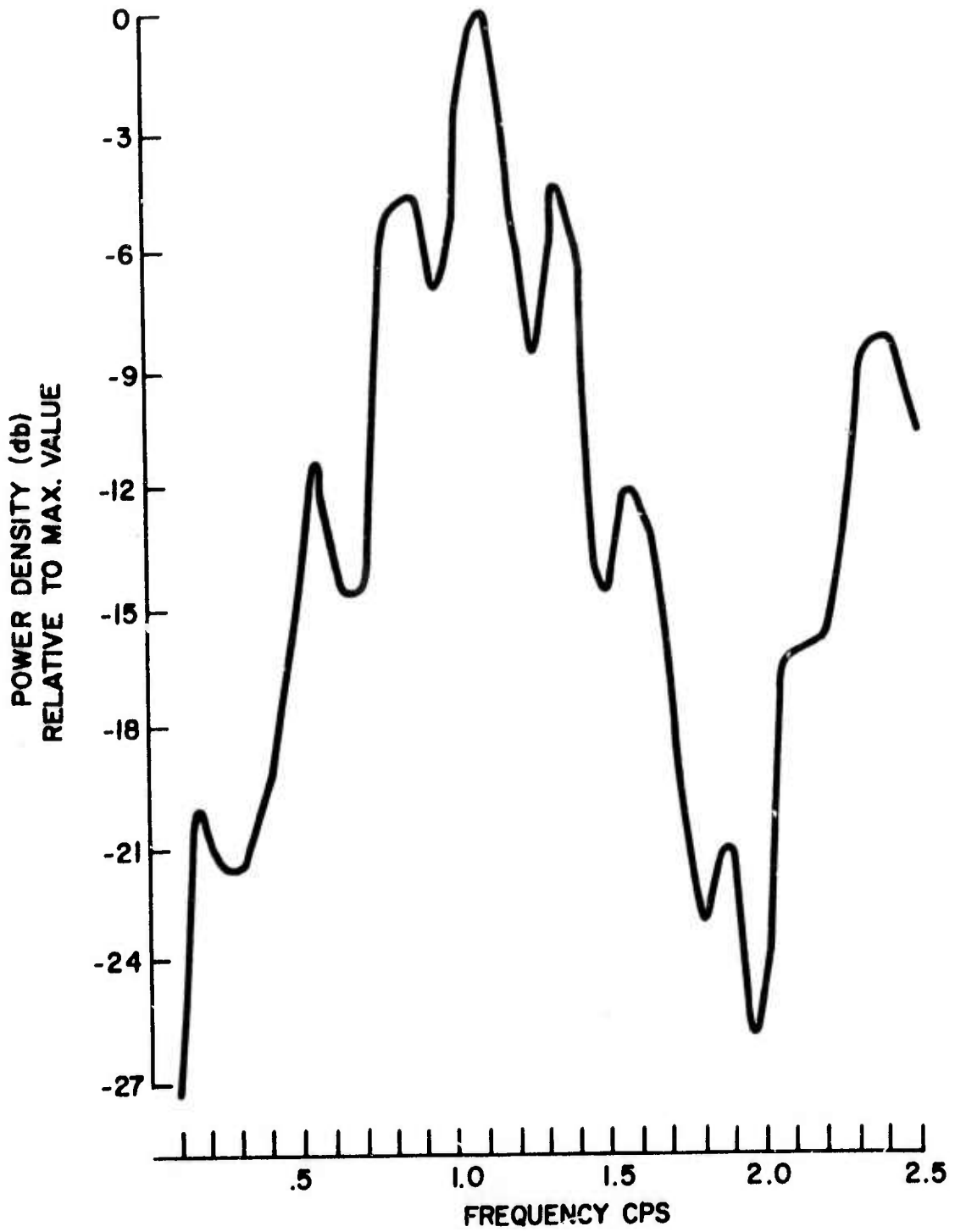


Figure 25. Beam-steered power-density spectrum of the LONG SHOT event at LASA Fl.

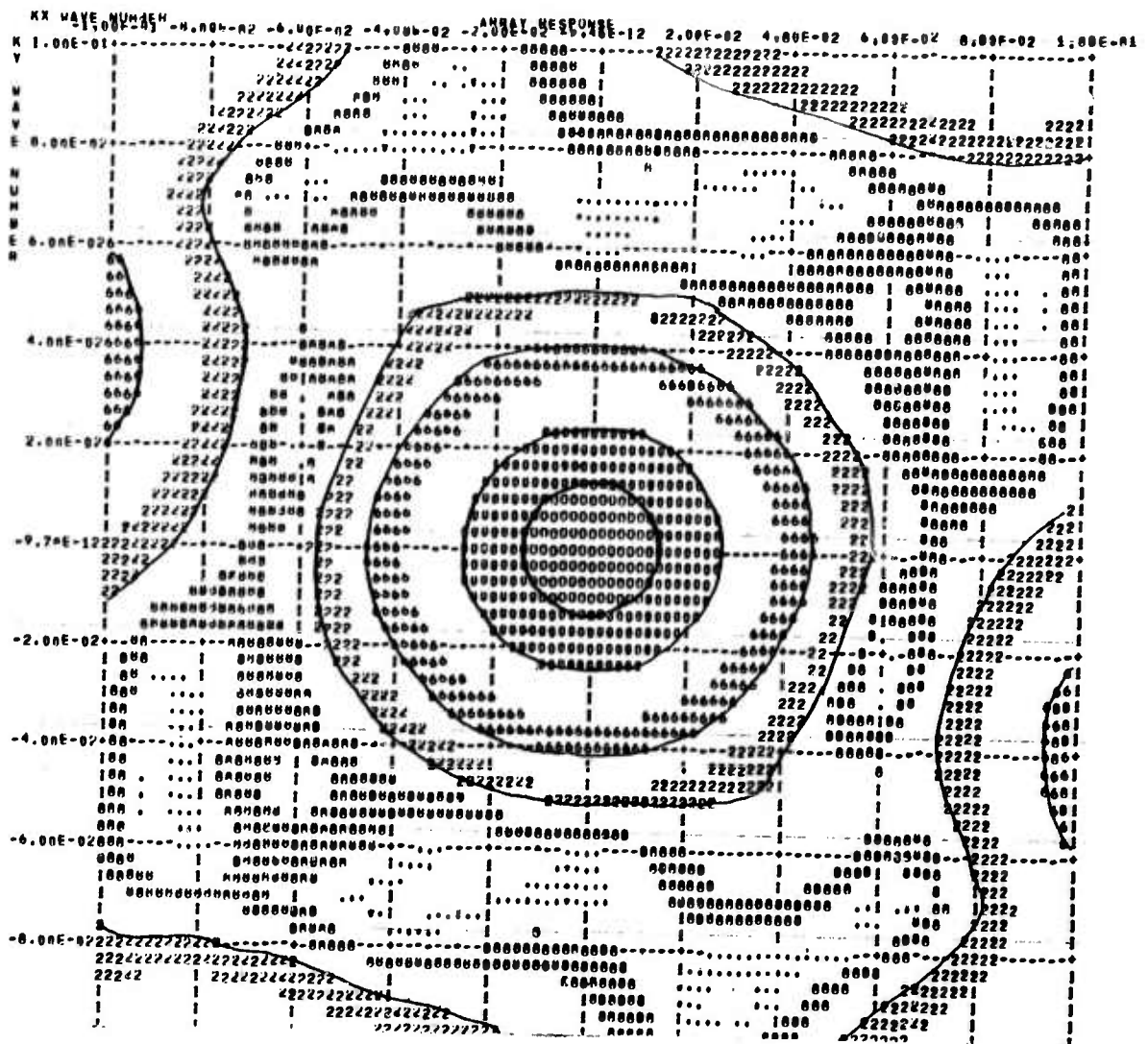


Figure 26. Array response of the partial XE3 array to an infinite velocity plane wave.

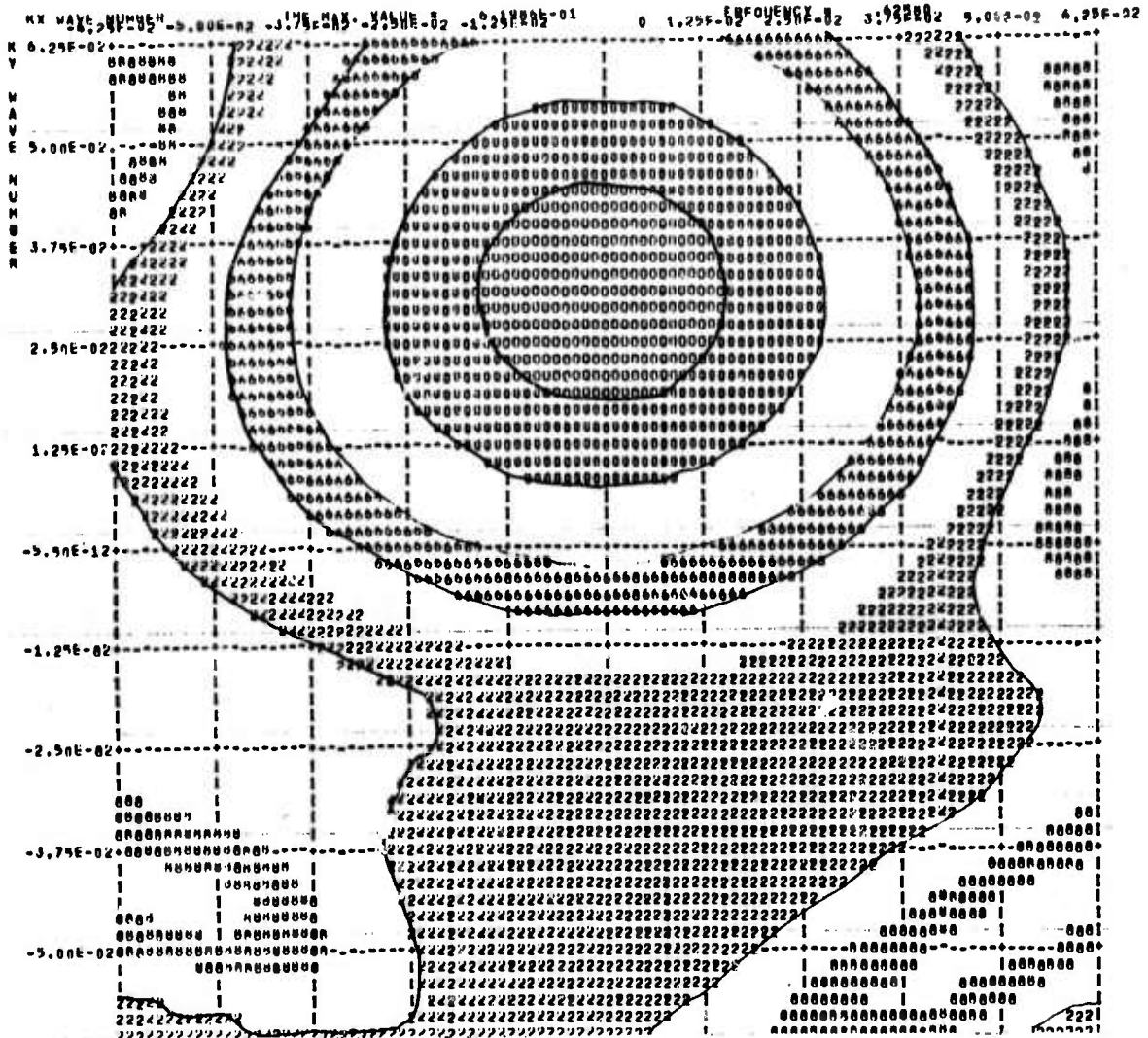


Figure 27. Ordinary f-k spectrum at .625 cps of two plane waves, one of amplitude 1 at 20 km/sec, North; and one of amplitude .2 at 30 km/sec, South.

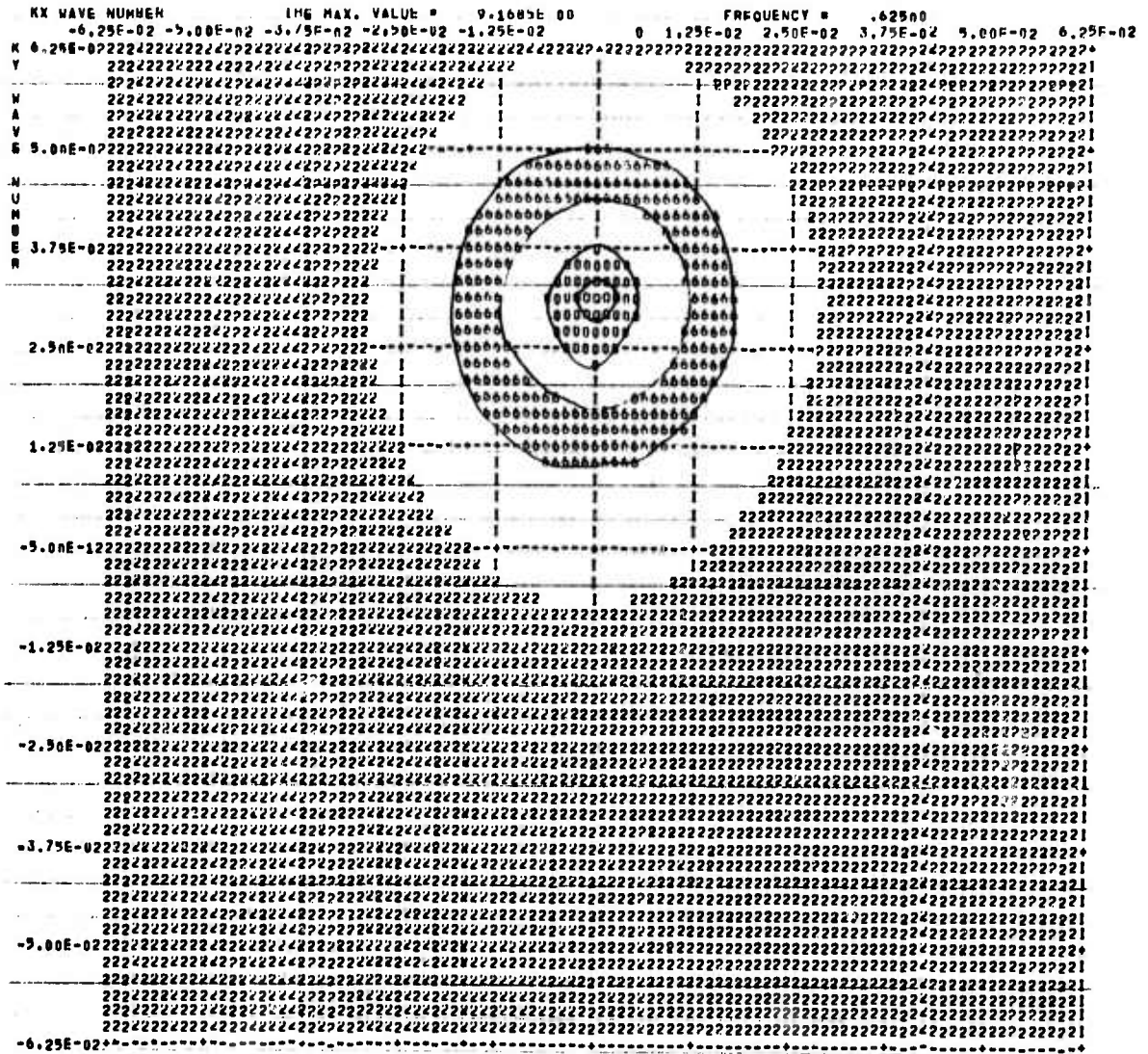


Figure 28. High-resolution wavenumber-spectrum of the two plane waves at .625 cps averaged over all of the sensors in the array S/N = 2.0.

at the same frequency. Figure 29 is the high-resolution f-k spectrum ($S/N = 0.03$) of the same event, calculated at the same frequency. At .625 cps the 30 km/sec event would not be detected by either the ordinary f-k spectrum (Figure 27) or by the average ($S/N = 2.0$) high-resolution f-k spectrum (Figure 28). The extreme elongation of the average ($S/N = 0.03$) high-resolution f-k spectrum (Figure 29) might make one suspicious about the presence of a second event, but the conclusion would depend on the subjective discrimination of the analyst.

We conclude from this investigation that although the high-resolution frequency-wavenumber spectrum gives much better resolution for single events, the technique does not improve significantly the capability of a seismic array to detect multiple time-overlapping events from different azimuths. A possible method of detecting a small event in the presence of a large event is to design an approximate pre-whitening filter in the time domain to approximately "whiten" the f-k spectrum of the data, convolve the filter with the time series data, and then proceed with either ordinary or high-resolution f-k analysis. The fact that the pre-whitening filter need be only an approximate whitening filter facilitates its design.

References

Burg, J.P., 1964, Three dimensional filtering with an array of seismometers: *Geophysics*, v. 29, p. 693-713.

Burg, J.P., 1967, Maximum-entropy spectral analysis: presented at the 37th annual meeting of the Society of Exploration Geophysicists.

Haney, W.P., 1967, Research on high-resolution frequency-wavenumber spectra, Special Scientific Report No. 2: Dallas, Texas Instruments, Inc., Contract AF33(657)-16678.

McCowan, D.W., 1966, Finite Fourier transform theory and its application to the computation of convolutions, correlations, and spectra, Seismic Data Laboratory Report No. 168 Revised: Alexandria, Virginia, Earth Sciences, A Teledyne Company.

McCowan, D.W. and Lintz, P.R., 1968, High-resolution frequency-wavenumber spectra, Seismic Data Laboratory Report No. 206, Alexandria, Virginia, Earth Sciences, A Teledyne Company.

E. Vertical Array Frequency-Wavenumber (v-f-k) Spectra of Synthesized Rayleigh Wave and P-Wave Noise.

In recent reports, Sax (1967) has discussed v-f-k (vertical array frequency-wave number) spectra of the noise fields preceding, underlying and following high frequency teleseismic P waves. In some cases, difficulties in relating v-f-k spectra of seismic data to wavemodes were encountered. Model studies are therefore undertaken in this study to investigate v-f-k patterns of synthesized Rayleigh wave and body wave noise. The purpose is to identify v-f-k patterns of synthesized Rayleigh wave and body wave noise. The purpose is to identify v-f-k patterns associated with random Rayleigh waves or body wave components.

McCowan (1968) described the method for computing v-f-k spectra. Harkrider's (1964) computer program was used to compute the Rayleigh wave modes described in the following results.

Figure 34 shows the geological structure used to compute the Rayleigh wave modes. The layering is characterized grossly by a halfspace velocity of 6 km/sec and interbedded 5.0 km/sec granite between 1.5 and 2.0 km. Only the

trapped modes produced by the interbedded low velocity zone are considered. Shear velocities were estimated by assuming a constant Poisson's ratio of .27.

Amplitude-depth curves of the vertical component of displacement are shown in Figure 30 for the fundamental mode; Figure 31, first higher mode; Figure 32, second higher mode; and Figure 33 the third higher mode. The low frequency limit of each propagation mode is determined by half-space radiation of modes with phase velocities greater than the shear velocity of a granite half-space.

The noise which was subjected to v-f-k analysis was synthesized by feeding random numbers into a set of constant-Q filters of .25 cps effective bandwidth. In order to cover a broad band of frequencies, the center frequency of each filter was spaced .25 cps apart starting at .25 cps and ending at 3.0 cps. An independent realization of random numbers was fed into each filter. The resultant broad band noise was the sum of the random uncorrelated outputs of each filter. The noise at the surface of the earth was normalized to be white, i.e., with a constant power spectrum. The simulated noise at depth, z_i , was multiplied by a coefficient corresponding to the n'th propagation mode $H_n(z_i, f_m)$ at each frequency, f_m . The band-limited wave components were summed over all the center frequencies, f_m , to obtain at each level, z_i , a broad band multichannel realization of noise in the n'th propagation mode. The noise is the convolution of a white random source $N'(t, f_m)$ with the response of a narrow band filter $F(t, f_m)$ which peaks at f_m . These narrowband realizations

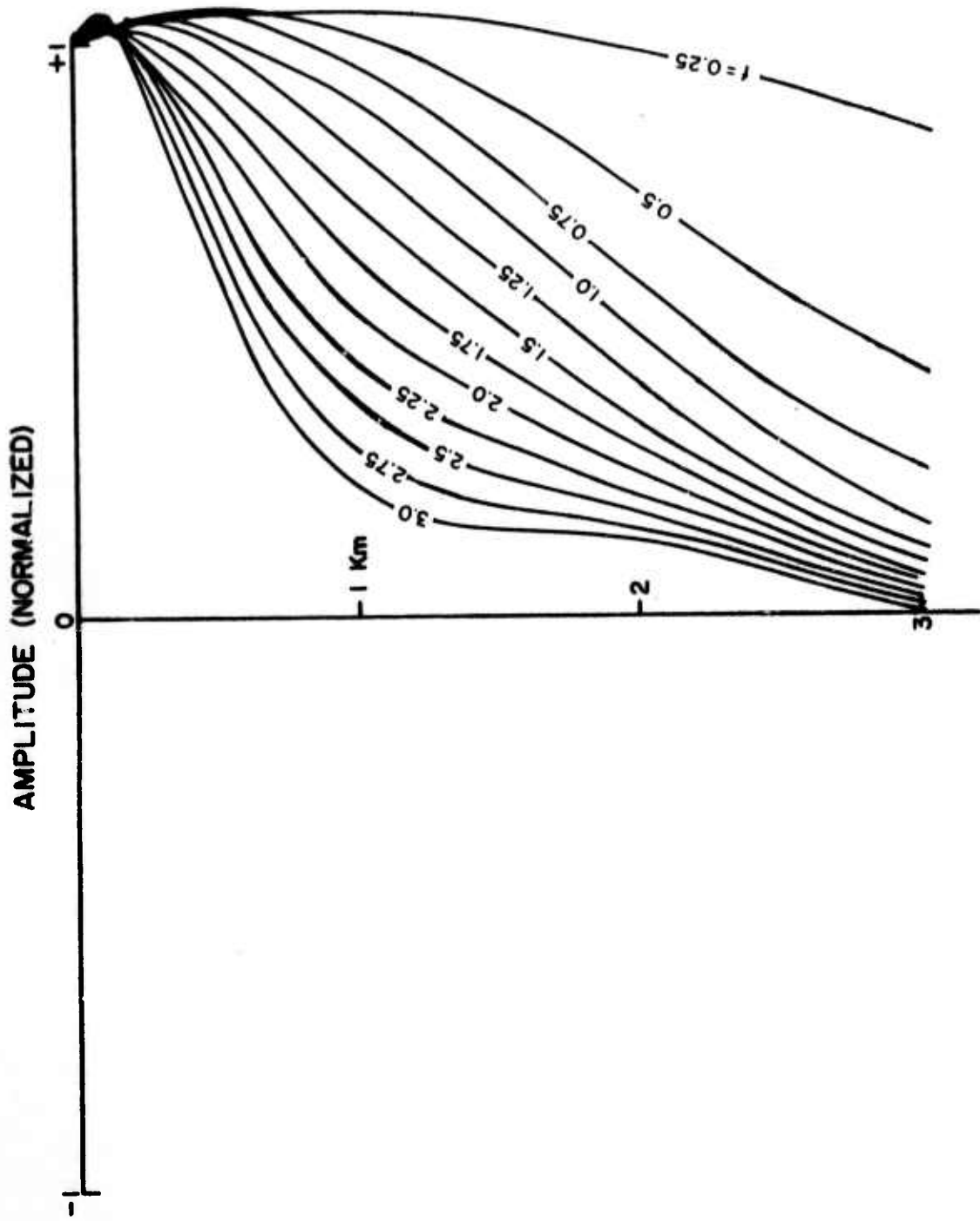


Figure 30. Frequency-Amplitude-Depth Relations
For Fundamental Rayleigh Mode at
Station APOK

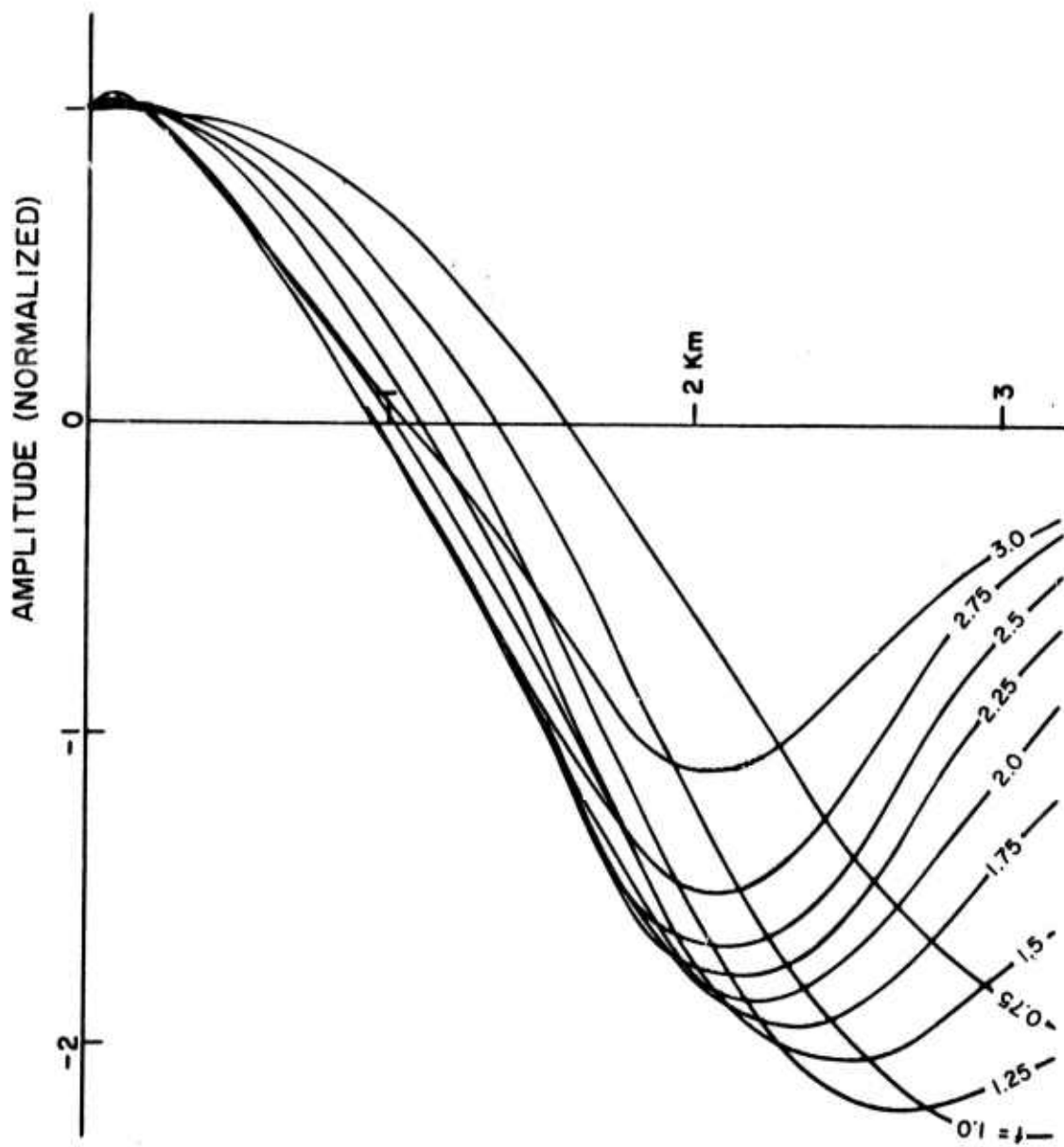


Figure 31. Frequency-Amplitude-Depth Relations For Higher Rayleigh Modes at Station APOK First Higher Mode

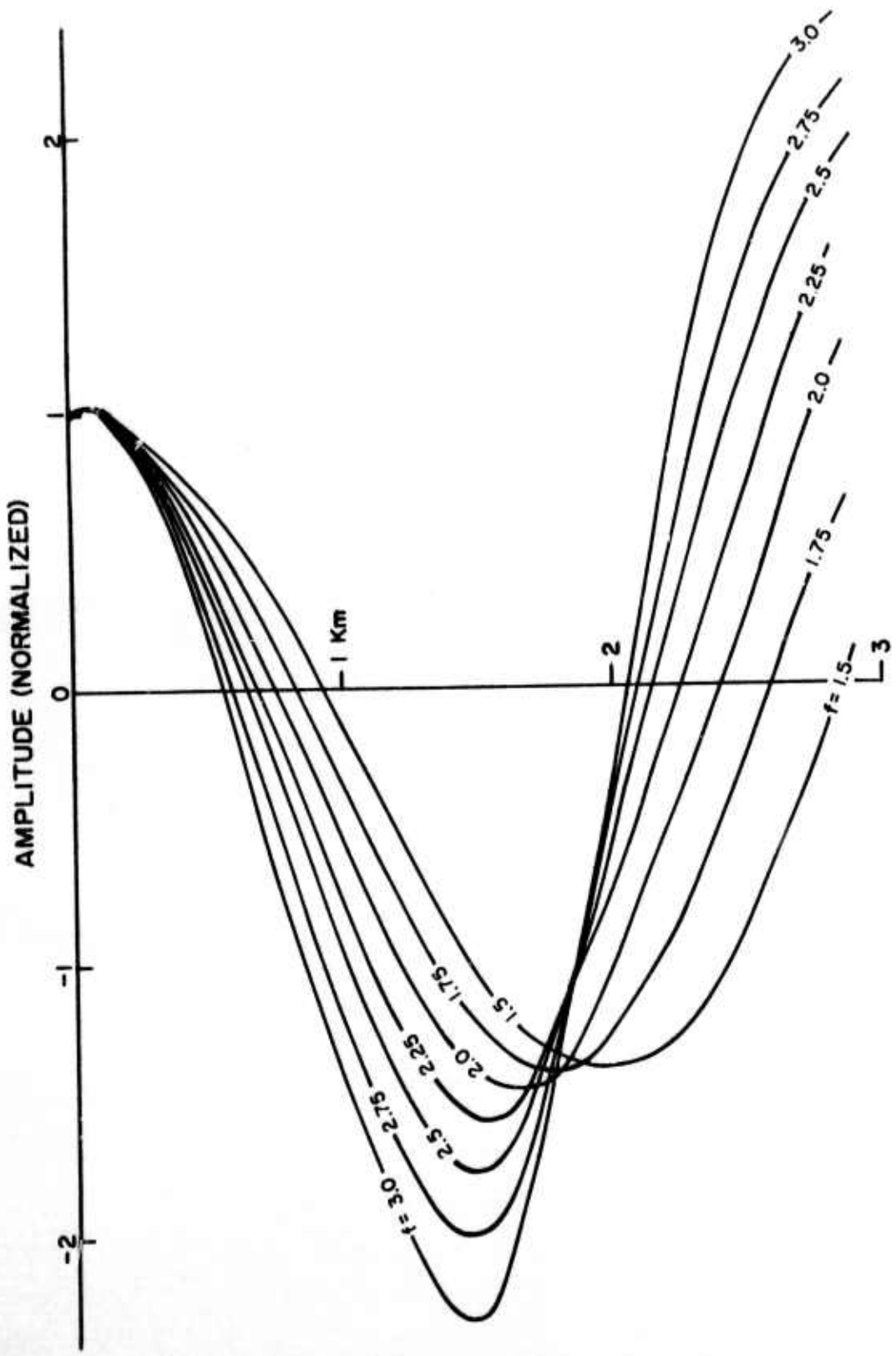


Figure 32. Frequency-Amplitude-Depth Relations For Higher Rayleigh Modes at Station APOK Second Higher Mode

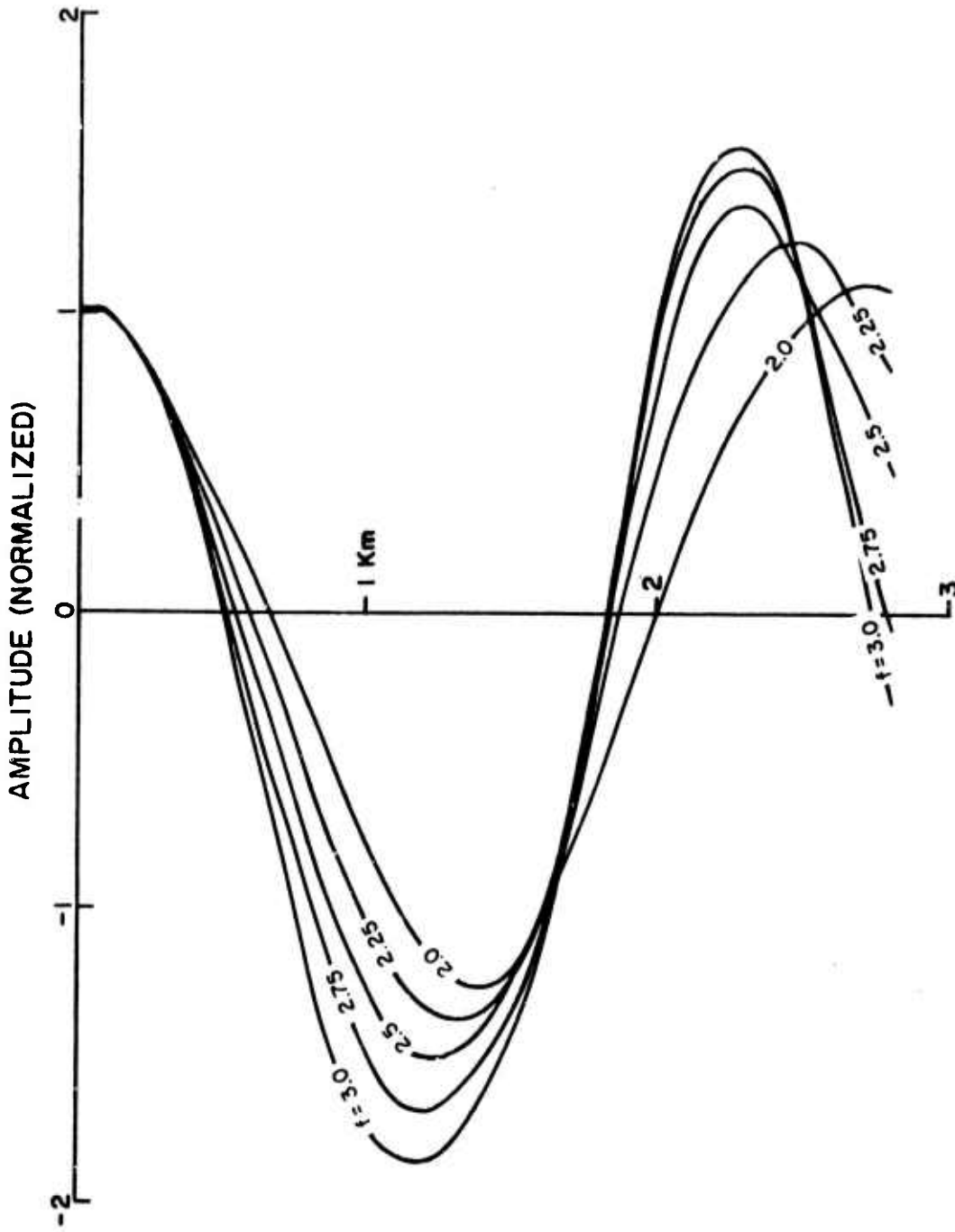


Figure 33. Frequency-Amplitude-Depth Relations
For Higher Rayleigh Modes at Station
APOK Third Higher Mode

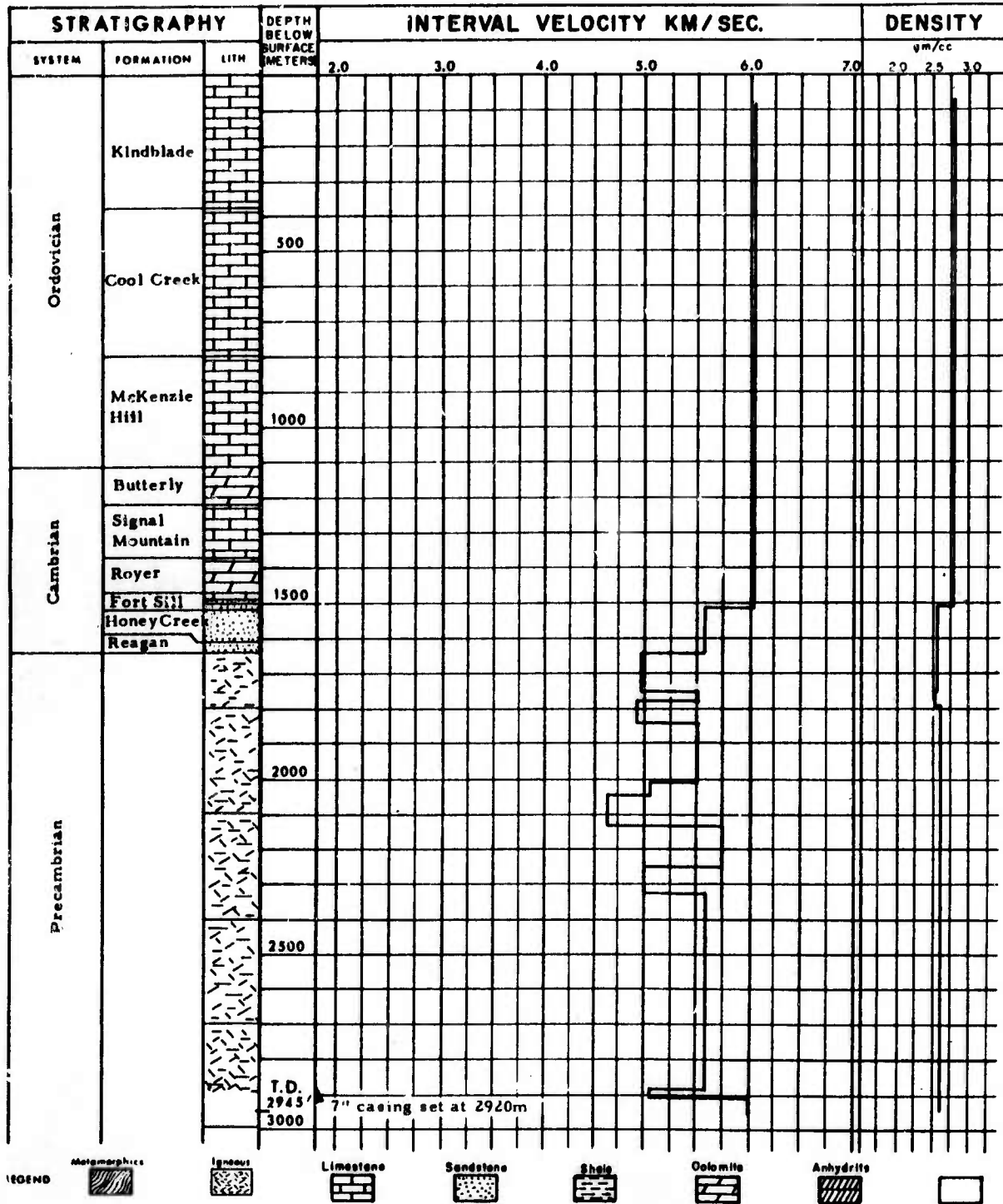


Figure 34. Velocity and Density Sections at Site APOK (Apache, Oklahoma)

are summed by weighting with $H_n(z_i, f_m)$, which for Rayleigh waves is previously cited. Similarly, body wave noise was synthesized by using the halfspace eigenfunction $\cos(2\pi f_m z_i/a)$, where a is the halfspace velocity of P-waves.

Figures 35-38 show the v-f-k spectra, for $k \geq 0$, for the four Rayleigh wave modes depicted in Figures 30 to 33. These are shown as if measured by a typical six-element vertical array approximately 3 km long, with each channel filtered by an operator which prewhitens the noise at the surface. The synthetic data were generated by means of a random number generating algorithm and narrow band filters as previously described. The synthetic data, if compared to observed data, are subject to the same array response, thereby eliminating some of the problems of array response implicit in the identification of waves. This follows as a consequence of using the same array geometry, sample size and rate, smoothing, etc., for both sets of data.

The amplitude spectra of the higher modes (Figures 36-38) are dominated by peaks at non-zero wave numbers running parallel to the frequency axis. This reflects a fixed number of zero crossings as a taper which splits the wave number response into two nearly parallel peaks similar to the way a cosine taper splits a dc time response into two discrete spectral peaks at the frequency of the taper. Compare the first, second, and third higher modes: the first higher mode is distinguishable on the basis of wave number splitting, but the second and third are indistinguishable from each other on this basis, having very similar v-f-k patterns. After comparing the displacement curves (Figures 32 and 33) for the second and third higher mode, we note that any apparent difference in wave number response is below the resolution of the v-f-k processor.

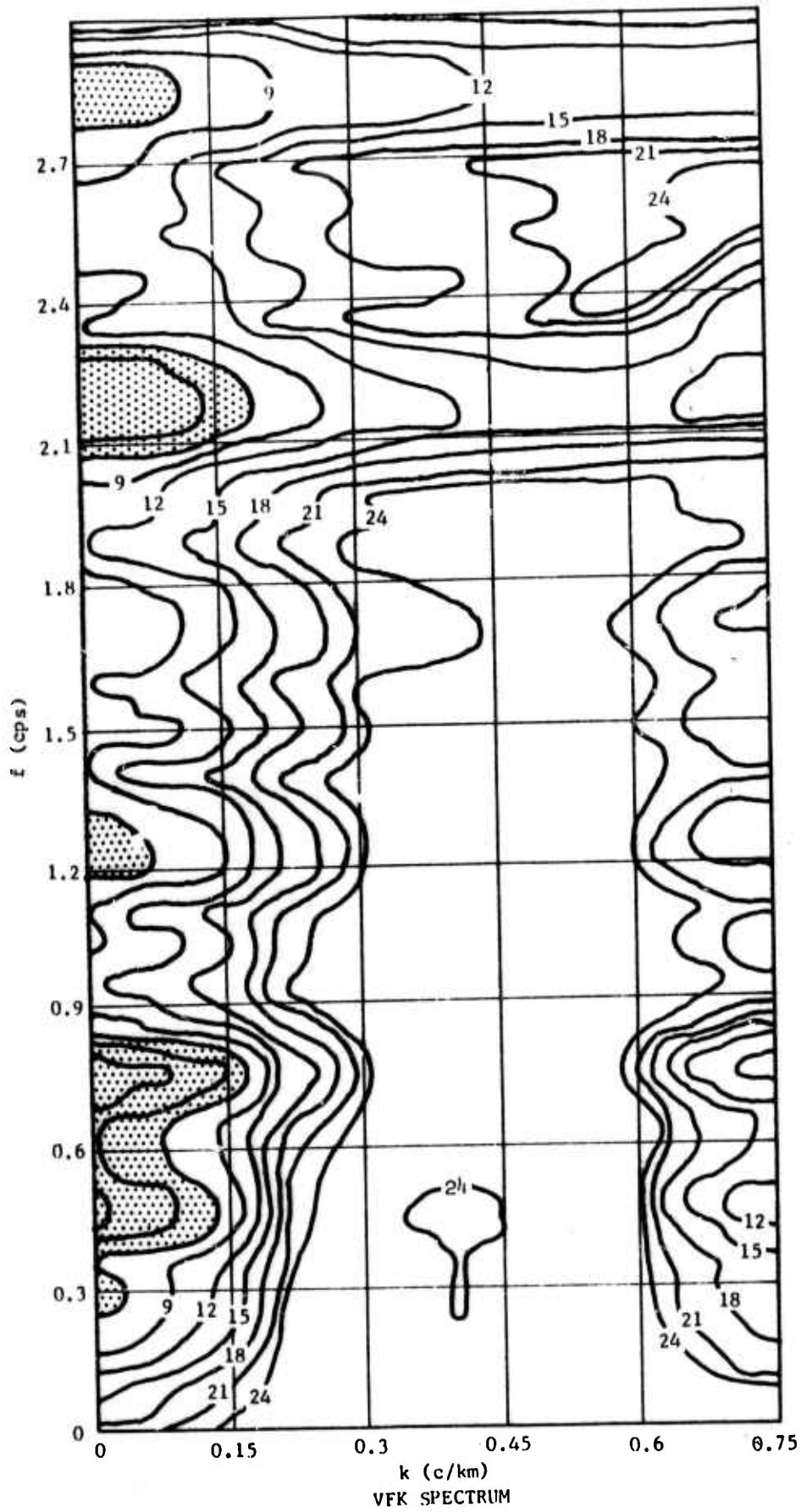


Figure 35. Fundamental Rayleigh Mode - Vertical Component - Station APOK

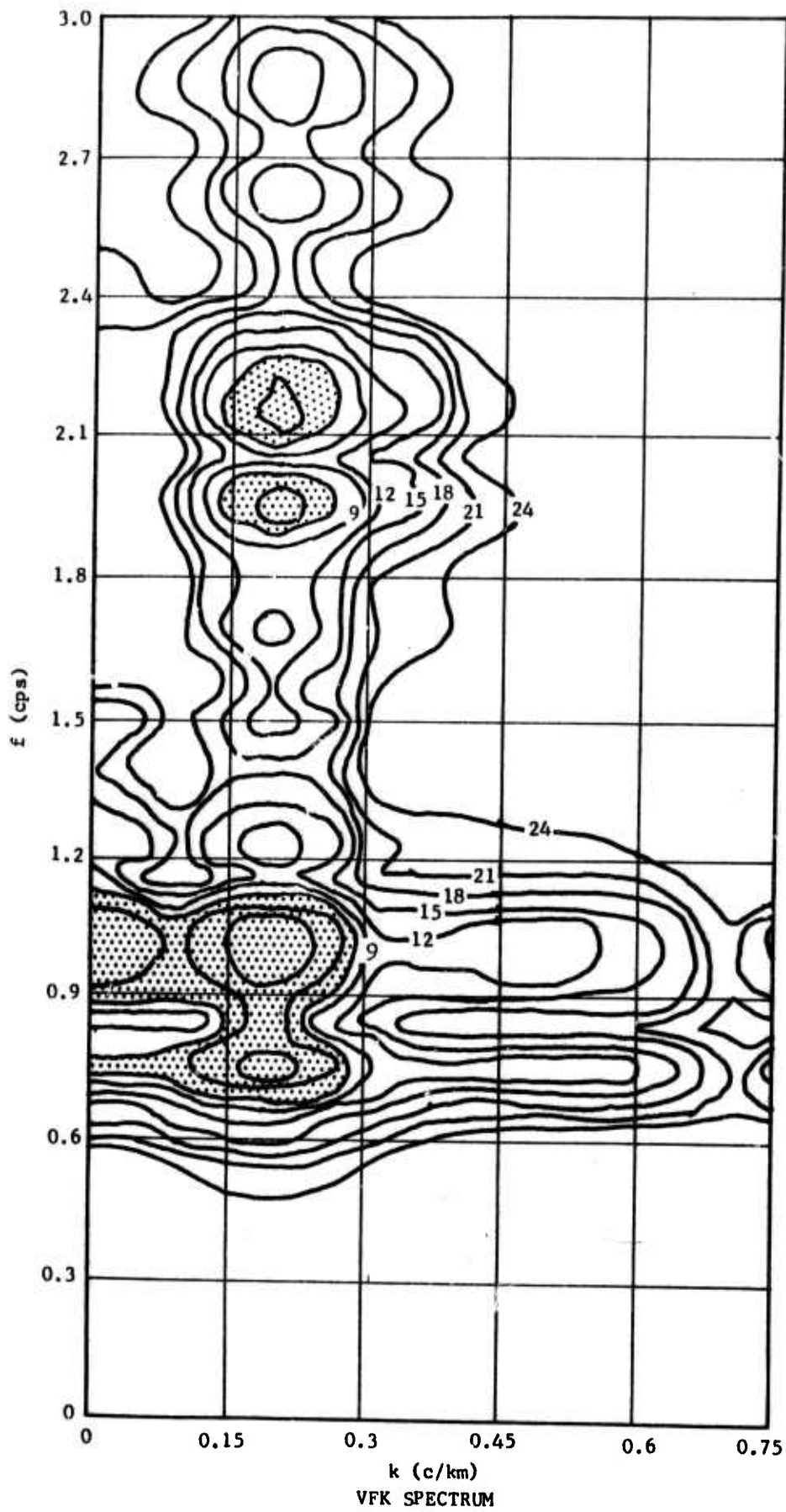


Figure 36. 1st Higher Rayleigh Mode - Vertical Component - Station APOK

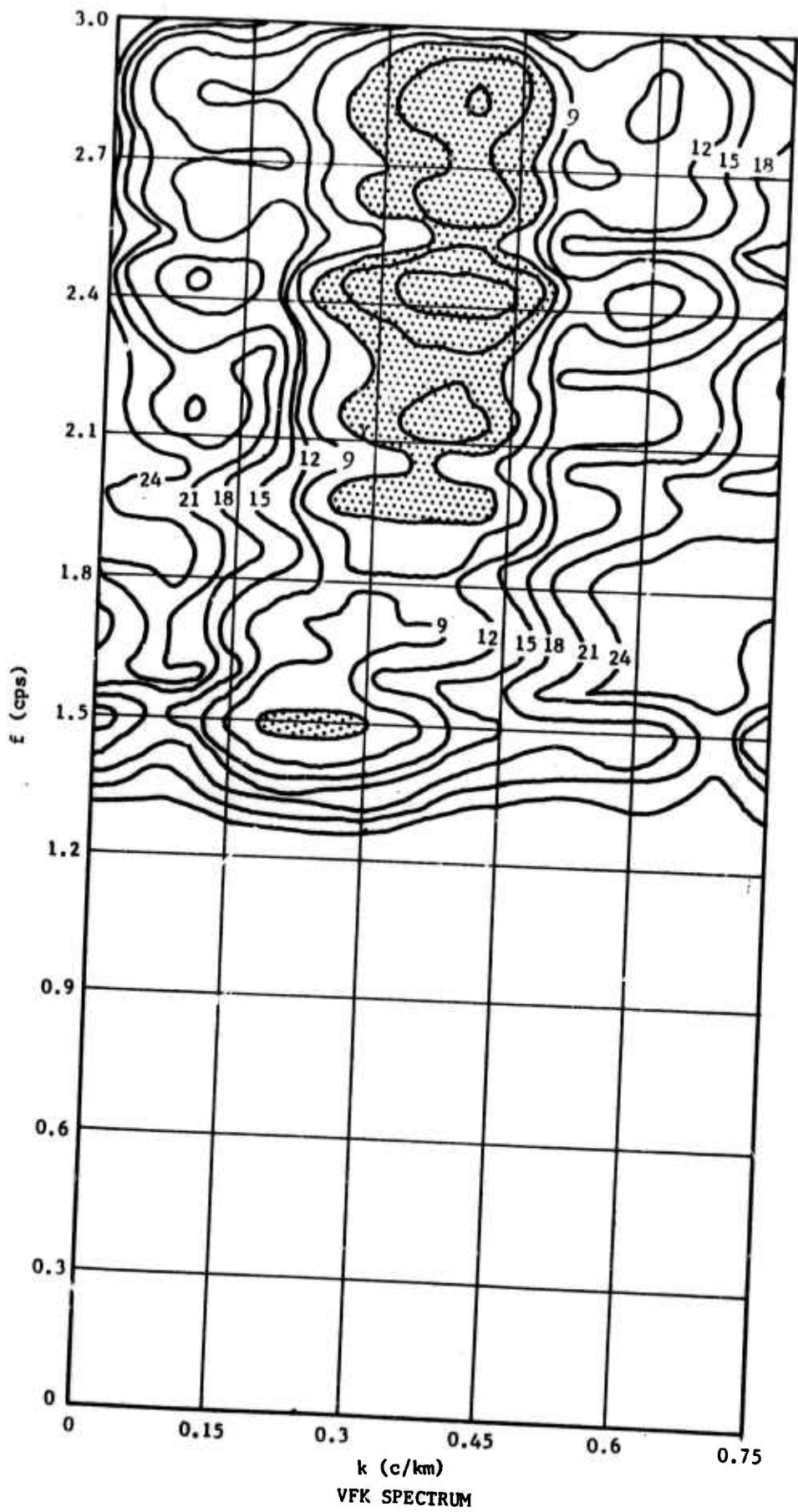


Figure 37. 2nd Higher Rayleigh Mode - Vertical Component - Station APOK

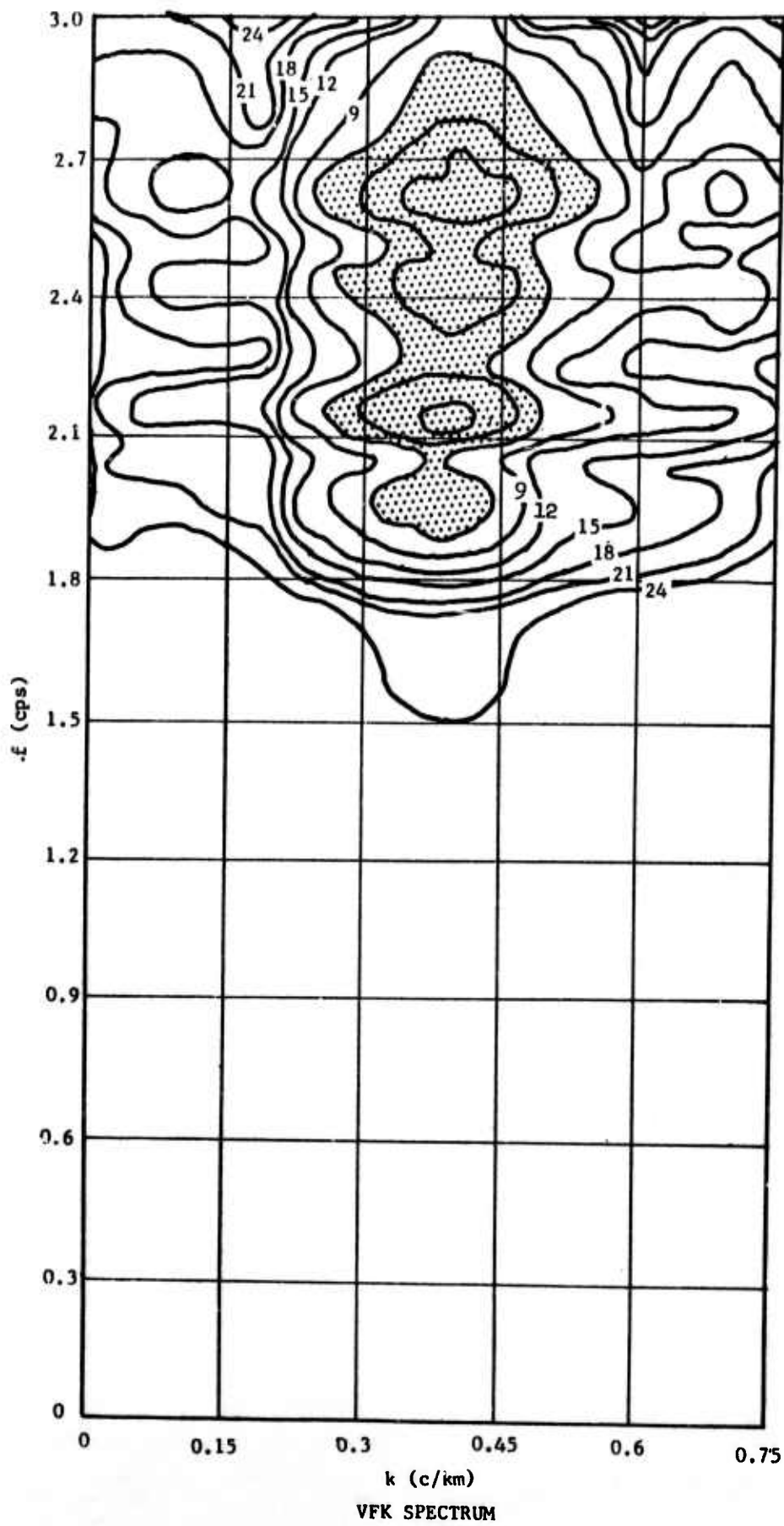


Figure 38. 3rd Higher Rayleigh Mode - Vertical Component - Station APOK

Figure 39 shows vertical P wave noise. The noise is generated by using the halfspace vertical displacement, $\cos 2\pi f x/a$, where a is an average halfspace compressional velocity. Figure 40 is the v - f - k spectrum corresponding to an up- and down-travelling impulse with the same average halfspace velocity used for Figure 39. In both cases, the shaded 3 db peaks indicate an apparent vertical phase velocity ($c = f/k = a$) corresponding to the average half-space velocity, a . The array responses differ considerably between the P impulse model of Figure 40 and the long random P wave function of Figure 39. The time series resulting in Figure 40 would be immediately obvious as a P impulse. The random time series resulting in Figure 39 looks almost totally incoherent between channels. It cannot be recognized as P noise unless we refer to Figure 39, in which case it is obvious.

Comparing the v - f - k analysis of higher modes on Figures 37 and 38 with the P noise on Figure 39, we see that P noise above 1.8 cps is barely distinguishable from the second and third higher mode Rayleigh waves. It is reasonable to anticipate some difficulty in designing filters to separate a narrow band-limited P signal from noise containing higher-mode Rayleigh waves. This result is significant, as it has been amply demonstrated that higher modes and possibly leaky modes and P waves are significant components of the ambient noise, especially above .5 cps.

The results of the study indicate that theoretical v - f - k analysis of wave modes should be extended to include deep crustal trapped modes which are almost certainly important components of ambient seismic noise. Further, high-resolution v - f - k analysis, McCowan and Lintz (1968), plus the aforementioned extended array concept could improve the array response due to sampling limitations imposed by the array geometry.

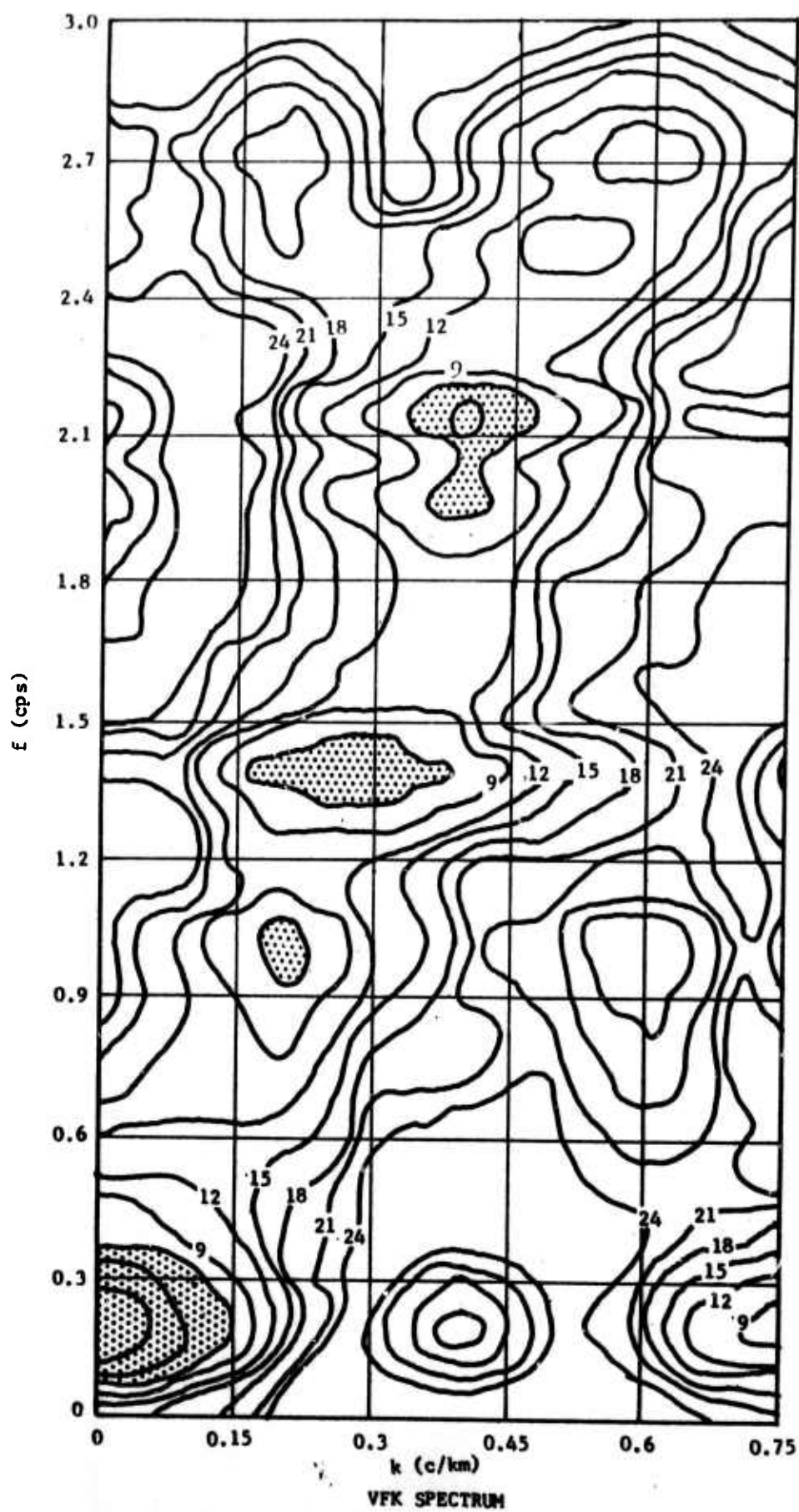


Figure 39. Teleseismic P-wave Noise - Vertical Component - Station APOK

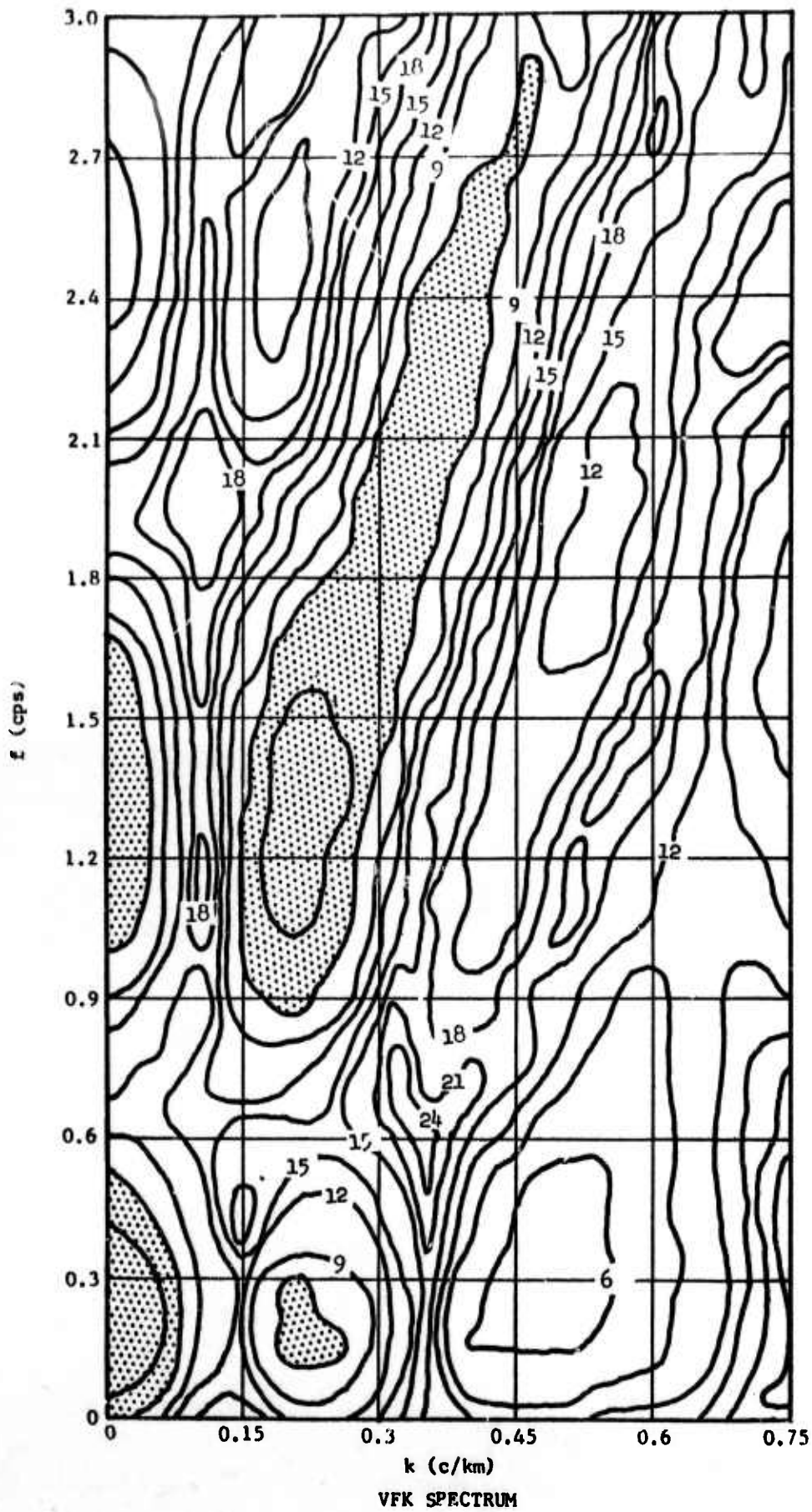


Figure 40. Teleseismic P-wave Signal (white)-
Vertical Component - Station APOK

F. Earthquake and Explosion Analysis

Standard statistical summary reports were issued on the Nevada Test Site nuclear events, SCROLL and BOXCAR. Table IX summarizes part of the seismic data compiled from these events.

Other projects completed included photo albums for two events and travel-time computations for NTS and other sites. In addition complexities were computed for a number of special events.

<u>Name</u>	<u>Event Date</u>	<u>Medium</u>	<u>Magnitude</u>	<u>No. of stations recording</u>	
				<u>SP Signals</u>	<u>LP Signals</u>
SCROLL	23 April 1968	Vitric Tuff	4.45 ± 0.44	18	6
BOXCAR	26 April 1968	Rhyolite	6.42 ± 0.45	23	22

TABLE IX. Seismic Data from Two Nuclear Explosions

III. SUPPORT AND SERVICE TASKS

A. VELA-Uniform Data Services

As part of the contract work statement, the SDL provided one or more of the following support and service functions for VSC and other VELA participants:

- copies of 16 and 35 mm film.
- playouts of earthquakes and special events.
- copies of composite analog tapes.
- composite analog tapes of special events.
- use of 1604 computer for checking out new programs or running production programs.
- copies of digital programs.
- digitized data in standard formats or special formats for use on computers other than the 1604.
- running SDL production programs, such as power spectral density and array processing on specified data.

- digital x-y plots of power spectra or digitized data.
- signal reproduction booklets.
- space for visiting scientists utilizing SDL facilities to study data and exchange information with SDL personnel.

During this report period, 56 such projects were completed and the 9 organizations receiving these services are listed in Appendix A.

B. Data Library

The data library contains approximately 8130 digitized seismograms, 237 digital computer programs and 298 composite analog magnetic tapes, all available for use by the VELA-Uniform program.

The following additions were made during this period:

1. Digital Seismograms - 730 including
 - data from two explosions
 - one earthquake recorded at various stations
2. LASA Data - 12 tapes
 - there are a total of 1408 digital tapes in the library including 1004 field tapes. There is also a master calibration tape which contains the magnification (digital counts per millimicron) of each sensor for every subarray. These magnifications have been computed for all calibration tapes currently in house. As each new calibration is received, it is routinely run through the new program CALIBR and added to the master tape.
3. Digital Programs - 12 including
 - SCRTAPE - To make and update BCD tapes containing standard production programs and subroutines.

COOLCEP - This program computes and displays power spectra and cepstra. A plot tape is generated with explanatory labels. Provision has been made for tapering and high-pass filtering (liftering) the power spectrum prior to computing the cepstrum. The Cooley-Tukey method is used to obtain high speed. The program is designed for multiple runs, reading data cards until and end-of-file is reached on the card reader.

BMSTR - Beamforms the data channels of an input seismogram and computes the power spectra from selected parts of the resulting trace.

BMSTEER - Generates a set of MCF beam-steer deltas and stores them on magnetic tape in a format suitable for processing by program M220 MCFONPT (revised). The time shifts are calculated geometrically from the array coordinates which are stored on tape and a velocity and back azimuth read in from cards.

MXTFOCAL - Computes magnification levels in counts/microns from the TFO calibration data on the original TFO acquisition system tape.

CALSETUP - This subroutine removes the mean and/or linear trend, finds the calibration and computes magnification level in counts/microns.

RESTRA - Determine the coefficients of the linear equation $y = a + Bx$ or alternately $\text{Log}(Z) = c + d \text{Log}(x)$. The user has the option to choose either equation. Moreover, the user can decide if correction factors are to be applied to the y's or the Log(Z)'s.

REGRESS - This program generates station correction factors which are used as input to program RESTRA.

PREFILT - This program writes a save tape of a MCF pre-filter suitable for processing by program M220 MCFONPT (revised). The prefilter coefficients are read from cards.

MULMATCH - Performs multichannel matched filtering on array data. The program produces printed and plotted outputs displaying the filter, the individual filtered traces, and the sum.

NORSARLP - Processes a Norsar tape (merged by Lincoln Laboratories) containing multiplexed long-period seismic data, and forms an unpacked SDL library tape.

GIVHOUSE - This Fortran-63 subroutine calculates the eigenvalues and eigenvectors of a real, symmetric matrix. The Givens-Householder method is used to reduce the matrix to a tri-diagonal form. The method of bisection is then used to obtain the eigenvalues and inverse iteration to obtain eigenvectors. The eigenvectors are normalized to have unit magnitude. An attempt is made to provide linearly-independent, but not necessarily orthonormal, eigenvectors for degenerate eigenvalues. Provision also exists to calculate less than the normal number of eigenvalues or eigenvectors. The eigenvalues are returned in order of decreasing magnitude.

4. Analog Composite Tapes - 5 including

a. Made by SDL

STUTZ
REX
RED HOT

b. Made by Geotech

KNOX
STINGER

C. Data Compression

This is a continuing routine operation, and production is maintained at the level needed to meet the requirements of the field operation (LRSM and U.S. Observatories) and the Seismic Data Laboratory. For this period 2100 tapes were compressed.

D. Automated Bulletin Process

April, May and June 1968 LRSM and Observatory Bulletins were processed during this report period and forwarded to Geotech, a Teledyne Company, for checking and publication.

APPENDIX A

April - June 1968

Organizations Receiving SDL Data Services

Vitro
General Atronics Corporation
Geotech, A Teledyne Company
Oregon State University
Texas A&M University
S.W. Center for Advanced Studies
U.S. Coast & Geodetic Survey
University of North Carolina
St. Louis University

DOCUMENT CONTROL DATA - R&D

(Security classification of title, body of abstract and indexing annotation must be entered when the overall report is classified)

1 ORIGINATING ACTIVITY (Corporate author) TELEDYNE, INC. ALEXANDRIA, VIRGINIA		2a REPORT SECURITY CLASSIFICATION Unclassified	
		2b GROUP	
3 REPORT TITLE SEISMIC DATA LABORATORY QUARTERLY TECHNICAL SUMMARY REPORT APRIL - JUNE 1968			
4 DESCRIPTIVE NOTES (Type of report and inclusive dates) Scientific			
5 AUTHOR(S) (Last name, first name, initial) Hartenberger, R.A.			
6. REPORT DATE 15 July 1968	7a. TOTAL NO. OF PAGES 91	7b. NO. OF REFS 12	
8a. CONTRACT OR GRANT NO. F 33657-68-C-0945	8b. ORIGINATOR'S REPORT NUMBER(S)		
b. PROJECT NO. VELA T/6702			
ARPA Order No. 624	8c. OTHER REPORT NO(S) (Any other numbers that may be assigned this report)		
ARPA Program Code No. 8F10			
10 AVAILABILITY/LIMITATION NOTICES This document is subject to special export controls and each transmittal to foreign governments or foreign nationals may be made only with prior approval of Chief, AFTAC.			
11 SUPPLEMENTARY NOTES		12. SPONSORING MILITARY ACTIVITY ADVANCED RESEARCH PROJECTS AGENCY NUCLEAR TEST DETECTION OFFICE WASHINGTON, D. C.	
13 ABSTRACT This report summarizes the work done by the SDL during the period April through June 1968, and is primarily concerned with seismic research activities related to the detection and identification of nuclear explosions and earthquake phenomenon. Also discussed are the support tasks and data services performed for other participants in the VELA-Uniform project.			
14 KEY WORDS Seismic Data Laboratory - Quarterly Technical Summary VELA-UNIFORM Project			